Multiple preferred escape trajectories are explained by a geometric model incorporating prey's turn and predator attack endpoint

Yuuki Kawabata[a,*], Hideyuki Akada[b], Ken-ichiro Shimatani[c], Gregory N. Nishihara[d], Hibiki Kimura[a], Nozomi Nishiumi[a,e], Paolo Domenici[f,g]

[a]*Graduate School of Fisheries and Environmental Sciences, Nagasaki University, 1-14 Bunkyo-machi, Nagasaki 852-8521, Japan*

[b]*Faculty of Fisheries, Nagasaki University, 1-14 Bunkyo-machi, Nagasaki 852-8521, Japan*

[c]*The Institute of Statistical Mathematics, 10-3 Midori-cho, Tachikawa, Tokyo 190-8562, Japan*

[d]*Institute for East China Sea Research, Organization for Marine Science Technology, Nagasaki University, 1551-7 Taira-machi, Nagasaki 851-2213, Japan*

[e]*National Institute for Basic Biology, 5-1 Higashiyama, Myodaiji, Okazaki, Aichi 444-8787, Japan.*

[f]*CNR-IAS, Località Sa Mardini, 09170, Torregrande, Oristano, Italy*

[g]*CNR-IBF, Area di Ricerca San Cataldo, Via G. Moruzzi N°1, 56124, Pisa, Italy.*

***Correspondence**: Yuuki Kawabata; Email: yuuki-k@nagasaki-u.ac.jp; Tel: +81-(0)95-819-2824

Abstract

The escape trajectory (ET) of prey – measured as the angle relative to the predator's approach path – plays a major role in avoiding predation. Previous geometric models predict a single ET; however, many species show highly variable ETs with multiple preferred directions. Although such a high ET variability may confer unpredictability to avoid predation, the reasons why animals prefer specific multiple ETs remain unclear. Here, we constructed a novel geometric model that incorporates the time required for prey to turn and the predator's position at the end of its attack. The optimal ET was determined by maximizing the time difference of arrival at the edge of the safety zone between the prey and predator. By fitting the model to the experimental data of fish *Pagrus major*, we show that the model can clearly explain the observed multiple preferred ETs. By changing the parameters of the same model within a realistic range, we were able to produce various patterns of ETs empirically observed in other species (e.g., insects and frogs): a single preferred ET and multiple preferred ETs at small (20–50°) and large (150–180°) angles from the predator. Our results open new avenues of

investigation for understanding how animals choose their ETs from behavioral and neurosensory perspectives.

Keywords: escape direction; escape response; escape turn; mathematical model; predator evasion

Introduction

When exposed to sudden threatening stimuli such as ambush predators, most prey species initiate escape responses that include turning swiftly and accelerating away from the threat. The escape responses of many invertebrate and lower vertebrate species are controlled by giant neurons that ensure a short response time [1]. Many previous studies have focused on two behavioral traits that are fundamental for avoiding predation: when to escape (i.e., flight initiation distance, which is measured as the distance from the predator at the onset of escape) and where to escape [i.e., escape trajectory (ET), which is measured as the angle of escape direction relative to the stimulus direction] [2]. Previous studies have investigated the behavioral and environmental contexts affecting these variables [3-8], because they largely determine the success or failure of predator evasion [9-13], and hence the fitness of the prey species. A large number of models on how animals determine their flight initiation distances have been formulated and tested by experiments [2]. Although a number of models have also been developed to predict animal ETs [4, 14, 15], there are still some unanswered questions about how the variability of the observed ETs is generated.

Two different escape tactics (and their combination) have been proposed to enhance the success of predator evasion [16, 17]: the optimal tactic (deterministic), which maximizes the distance between the prey and the predator (Figure 1A) [4, 14, 15, 18], and the protean tactic (stochastic), which maximizes unpredictability to prevent predators from adjusting their strike trajectories accordingly (Figure 1B) [19-22]. Previous geometric models, which formulate optimal tactics, predict a single ET that depends on the relative speeds of the predator and the prey [4, 14, 15, 18], and additionally, predator's turning radii and sensory-motor delay in situations where the predator can adjust its strike path [23-25]. The combination of the optimal tactic (formulated by previous geometric models), which predicts a specific single ET, and the protean tactic, which predicts variability, can explain the ET variability within a limited angular sector that includes the optimal ET (Figure 1C). However, the combination of the two tactics cannot explain the complex ET distributions reported in empirical studies on various taxa of invertebrates and lower vertebrates (reviewed in [26]). Whereas some animals exhibit unimodal ET patterns that satisfy the prediction of

the combined tactics or optimal tactic with behavioral imprecision (e.g., [27]), many animal species show multimodal ETs within a limited angular sector (esp., 90–180°) (Figure 1D) (e.g., [4, 5, 28]). To explore the discrepancy between the predictions of the models and empirical data, some researchers have hypothesized mechanical/sensory constraints [17, 29]; however, the reasons why certain animal species prefer specific multiple ETs remain unclear.

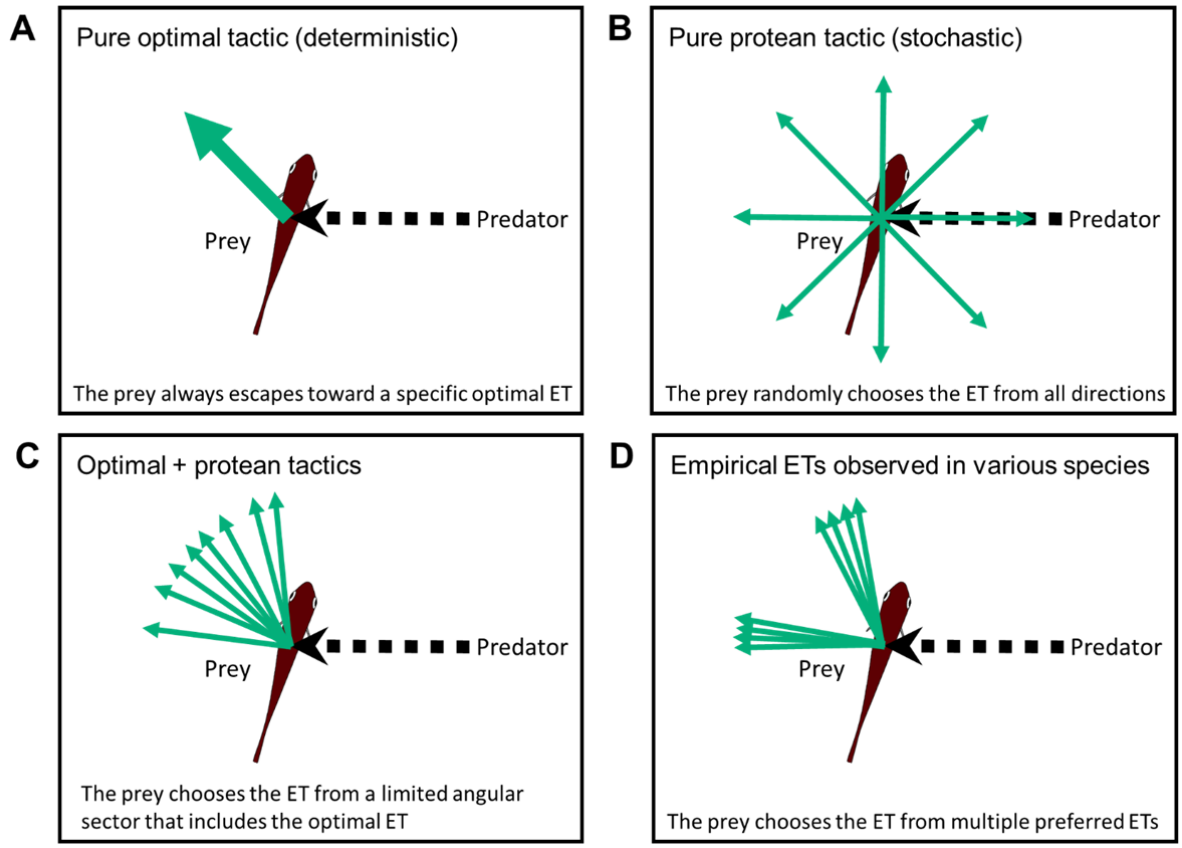

Figure 1. Conceptual diagram showing the different tactics for escape trajectories (ETs). (A) The pure optimal tactic, which predicts a specific optimal ET. (B) The pure protean tactic, which predicts a random ET from all directions. (C) The combination of optimal and protean tactics, which predicts an ET selected randomly (or with a specific probability distribution) from a limited angular sector that includes the optimal ET. (D) The multiple preferred ETs, empirically observed in various species. Please also see Domenici et al. [17] for the review on potential ETs.

Multiple preferred ETs of prey can result from situations in which animals choose one behavior from multiple options. Previous work carried out in the field of human and animal psychology on the choice of a particular behavioral strategy out of a number of options, has proposed a principle called “matching law.” According to this principle, the probability of a certain behavior to occur is related to the proportion of rewards obtained [30-33]. This is in contrast to a purely optimal

tactic, where animals should always choose the best option (i.e., the highest rewards obtained) [33, 34]. Arguably, the field of predator-prey interactions has the potential to benefit from an analytical interpretation based on the matching law, because the multiple ETs available to the prey set a scenario similar to the multiple behavioral options considered in previous work analyzed using this principle. In line with this approach, the probability with which a prey chooses a particular escape trajectory can be related to the rewards (chances of survival) of each ET option calculated from a predator-prey geometric model.

In previous geometric models, the prey was assumed to instantaneously escape in any direction, irrespective of the prey's initial body orientation relative to the predator's approach path (hereafter, initial orientation) [4, 14, 15]. However, additional time is required for changing the heading direction (i.e., turn); therefore, a realistic model needs to take into account that the predator can approach the prey while the prey is turning [12]. Additionally, in previous models, attacking predators were assumed to move for an infinite distance at a constant speed [4, 14, 15]. However, the attacks of many real predators, especially ambush ones, end at a certain distance from initial positions of the prey [35-37]. Therefore, we constructed a geometric model that incorporates two additional factors: the time required for the prey to turn and the endpoint of the predator attack. First, using a fish species as a model, we tested whether our model could predict empirically observed multimodal ETs. Second, by calculating the chances of survival of each ET option from our model, we investigated how the prey fish chose a given ET from multiple options. Third, by extending the model, we tested whether other patterns of empirical ETs could be predicted: unimodal ETs and multimodal ETs directed at small (20–50°) and large (150–180°) angles from the predator's approach direction. The biological implications resulting from the model and experimental data are then discussed within the frameworks of predator-prey interactions and behavioral decision-making.

Model

We revised the previous model proposed by Domenici [15, 38] (Figure 2A) (and the model proposed by Corcoran & Conner [24], Appendix 1—figure 1A). Other previous models [4, 14, 18, 25] made predictions similar to those of Domenici's model or those of Corcoran's model, although they used different theoretical approaches. In Domenici's model, the predator with a certain width (i.e., the width of a killer whale's tail used as a weapon to catch prey) directly approaches the prey, and the prey (the whole body) should enter the safety zone before the predator reaches that entry point. In

this model, the prey can instantaneously escape in any direction, and the predation threat moves linearly and infinitely. Corcoran's model is based on the same principle as Domenici's model, but includes the concept that the predator (i.e., a bat) can adjust the approach path up to its minimum turning radius. Thus, Domenici's model can be regarded as a special case of Corcoran's model when the turning radius of the predator is infinitely large. These models are based on the escape response of the horizontal plane, which is realistic for many fish species as well as terrestrial and benthic species that move on substrates. They can also be applied to aerial animals such as moths escaping from bats because many predator-prey interactions are approximately two-dimensional in a local spatial scale [24, 39]. Hereafter, we explain the modification of Domenici's model (a special case of Corcoran's model) because the data on previously published predator-prey experiments on the same species of prey and predator in our experiment [12] show that the predator does not adjust the strike path during the attack [Figure 2—figure supplement 1, adjusted angle=1.0±6.6° (mean±s.d.), n=5], and thus the number of parameters to estimate can be reduced. See Appendix 1 for details of the modified version of Corcoran's model.

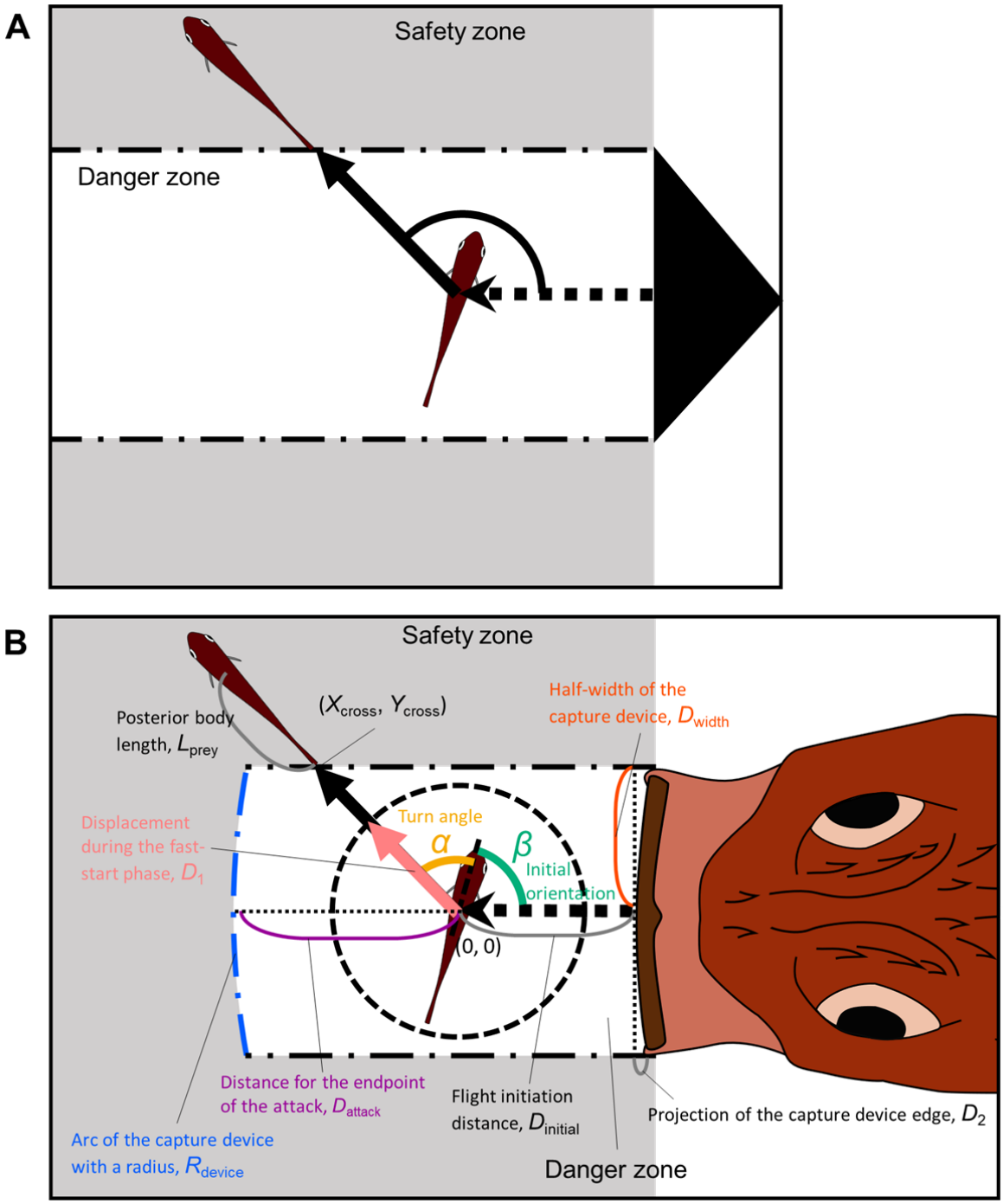

Figure 2. Proposed geometric models for animal escape trajectories. (A) A previous geometric model proposed by Domenici [15]. The predation threat with a certain width (the tail of a killer whale, represented by the black triangle) directly approaches the prey, and the prey should reach the safety zone (a grey area) outside the danger zone (white area) before the threat reaches that point. In this model, the prey can instantaneously escape in any direction, and the predation threat moves linearly and infinitely. (B) Two factors are added to Domenici's model: the endpoint of the predator attack, and the time required for the prey to turn. (X_{cross}, Y_{cross}) denotes the x and y coordinates of the crossing point of the escape path and the safety zone edge.

Figure supplement 1. Schematic drawing of how the adjusted angle of the predator (θ) was measured.

Figure supplement 2. Schematic drawing of angular variables.

In our new model (Figure 2B), two factors are added to the previous Domenici's model: the time required for the prey to turn and the endpoint of the predator attack. We assume that a prey with a certain initial orientation β (spanning 0–180°, where 0° and 180° correspond to being attacked from front and behind, respectively) evades a sudden predation threat. Most prey species respond to the attack by turning at an angle α, and the ET results from the angular sum of α and β. ETs from the left and right sides were pooled and treated as though they were stimulated from the right side (Figure 2—figure supplement 2; See "Definition of the Angles" in Materials and Methods for details).

When the prey's center of mass (CoM) at the onset of its escape is located at point (0, 0), the trajectory of the CoM ($X_{\mathrm{prey}},\ Y_{\mathrm{prey}}$) is given by:

$$\boldsymbol{Y_{prey} = X_{prey} \tan(\alpha + \beta)} \quad [1]$$

The edge of the safety zone is determined by the half-width of the predator capture device (e.g., mouth) D_{width}, the distance between the prey's initial position and the tip of the predator capture device at the end of the predator attack D_{attack}, and the shape of the predator's capture device at the moment of attack, which is approximated as an arc with a certain radius, R_{device}. The projection of the predator's capture device edge along the edge of the sideways safety zone D_2 can be expressed as:

$$\boldsymbol{D_2 = R_{device}\{1 - \cos(\sin^{-1}\frac{D_{width}}{R_{device}})\}} \quad [2]$$

The ET toward the upper-left corner of the danger zone θ_{corner} can be expressed as:

$$\boldsymbol{\theta_{corner} = \tan^{-1}\frac{D_{width}}{D_2 - D_{attack}}} \quad [3]$$

The x and y coordinates of the safety zone edge ($X_{\mathrm{safe}},\ Y_{\mathrm{safe}}$) are given by:

$$\begin{cases} \boldsymbol{Y_{safe} = D_{width}, \alpha + \beta < \theta_{corner}} \\ \boldsymbol{(X_{safe} + D_{attack} - R_{device})^2 + Y_{safe}{}^2 = R_{device}{}^2, \alpha + \beta \geq \theta_{corner}} \end{cases} \quad [4]$$

From equations [1] to [4], the x and y coordinates of the crossing point of the escape path and the safety zone edge ($X_{\mathrm{cross}},\ Y_{\mathrm{cross}}$) are given by a function of D_{width}, D_{attack}, R_{device}, and α+β.

The prey can escape from the predator when the time required for the prey to enter the safety zone (T_{prey}) is shorter than the time required for the predator's capture device to reach that entry point (T_{pred}). Therefore, the prey is assumed to maximize the difference between the T_{pred} and T_{prey} (T_{diff}). To incorporate the time required for the prey to turn, T_{prey} was divided into two phases: the fast-start phase, which includes the time for turning and acceleration (T_1), and the constant speed phase (T_2). This assumption is consistent with the previous studies [40-42] and was supported by our experiment (See Figure 4—figure supplement 1). Therefore:

$$\boldsymbol{T_{prey} = T_1 + T_2} \quad [5]$$

For simplicity, the fish was assumed to end the fast-start phase at a certain displacement from the initial position in any α (D_1; the radius of the dotted circle in Figure 2B) and to move at a constant speed U_{prey} to cover the rest of the distance (toward the edge of the safety zone $\sqrt{{X_{cross}}^2 + {Y_{cross}}^2} - D_1$, plus the length of the body that is posterior to the center of mass L_{prey}). Because a larger $|\alpha|$ requires further turning prior to forward locomotion, which takes time [40, 43], and the initial velocity after turning was dependent on $|\alpha|$ in our experiment (See Figure 4B), T_1 is given by a function of $|\alpha|$ [$T_1(|\alpha|)$]. Therefore, T_{prey} can be expressed as:

$$\boldsymbol{T_{prey} = T_1(|\alpha|) + \frac{\sqrt{{X_{cross}}^2 + {Y_{cross}}^2} - D_1 + L_{prey}}{U_{prey}}} \quad [6]$$

T_{pred} can be expressed as:

$$\boldsymbol{T_{pred} = \begin{cases} \frac{D_{initial} + D_2 - X_{cross}}{U_{pred}}, \alpha + \beta < \theta_{corner} \\ \frac{D_{initial} + D_{attack}}{U_{pred}}, \alpha + \beta \geq \theta_{corner} \end{cases}} \quad [7]$$

where $D_{initial}$ is the distance between the prey and the predator at the onset of the prey's escape response (i.e., the flight initiation distance or reaction distance), and U_{pred} is the predator speed, which is assumed to be constant. From equations [5] to [7], T_{diff} can be calculated as:

$$\boldsymbol{T_{diff} =} \quad [8]$$

$$\boldsymbol{\begin{cases} \frac{D_{initial}}{U_{pred}} + \frac{D_2}{U_{pred}} - \frac{X_{cross}}{U_{pred}} - T_1(|\alpha|) - \frac{\sqrt{{X_{cross}}^2 + {Y_{cross}}^2}}{U_{prey}} + \frac{D_1}{U_{prey}} - \frac{L_{prey}}{U_{prey}}, \alpha + \beta < \theta_{corner} \\ \frac{D_{initial}}{U_{pred}} + \frac{D_{attack}}{U_{pred}} - T_1(|\alpha|) - \frac{\sqrt{{X_{cross}}^2 + {Y_{cross}}^2}}{U_{prey}} + \frac{D_1}{U_{prey}} - \frac{L_{prey}}{U_{prey}}, \alpha + \beta \geq \theta_{corner} \end{cases}}$$

Because $\frac{D_{initial}}{U_{pred}} + \frac{D_1}{U_{prey}} - \frac{L_{prey}}{U_{prey}}$ are independent of α and β, we can calculate the relative values of T_{diff} (T_{diff}') in response to the changes of α and β, from:

$$\boldsymbol{T_{diff}' = \begin{cases} \frac{D_2}{U_{pred}} - \frac{X_{cross}}{U_{pred}} - T_1(|\alpha|) - \frac{\sqrt{{X_{cross}}^2 + {Y_{cross}}^2}}{U_{prey}}, \alpha + \beta < \theta_{corner} \\ \frac{D_{attack}}{U_{pred}} - T_1(|\alpha|) - \frac{\sqrt{{X_{cross}}^2 + {Y_{cross}}^2}}{U_{prey}}, \alpha + \beta \geq \theta_{corner} \end{cases}} \quad [9]$$

Because X_{cross} and Y_{cross} are dependent on D_{width}, D_{attack}, and R_{device} as well as $\alpha+\beta$, and D_2 is dependent on D_{width} and R_{device}, we can calculate $T_{\mathrm{diff}}{}'$ in response to the changes of α and β, from D_1, D_{width}, D_{attack}, R_{device}, U_{prey}, U_{pred}, and $T_1(|\alpha|)$. Given that the escape success is assumed to be dependent on $T_{\mathrm{diff}}{}'$, the theoretically optimal ET can be expressed as:

$$\textbf{The optimal ET} = \underset{\alpha+\beta}{\textbf{argmax}}(\boldsymbol{T_{\mathrm{diff}}{}'}) \qquad [10]$$

Results

Experimental Results. *P. major* exhibited a typical C-start escape response (Figure 2—figure supplement 2; Figure 3—figure supplement 1), which consists of the initial bend (stage 1), followed by the return tail flip (stage 2), and continuous swimming or coasting (stage 3) [44, 45]. Figure 3 shows the effect of the initial orientation β on the ETs. As was done in previous studies [26, 46, 47], the away (contralateral) and toward (ipsilateral) responses, defined as the first detectable movement of the fish oriented either away from or toward the predator, were analyzed separately. When the initial orientation was small (i.e., the prey was attacked head-on; Figure 3A; $0°\leq\beta<30°$), two peaks in the ET distribution were observed: a larger peak at around 100° (away response) and a smaller one at around −80° (toward response). As the initial orientation increases (Figure 3A; $30°\leq\beta<60°$), the peak at around −80° disappeared. As the initial orientation further increases beyond 60°, another peak appeared at around 170° (Figure 3A). When the initial orientation was large (i.e., the prey was attacked from behind; Figure 3A; $150°\leq\beta\leq180°$), there were two similar-sized peaks in the ET at around 130° (toward response), and 180–200° (away response). There were significant effects of initial orientation on the ET in both the away and the toward responses [away: generalized additive mixed model (GAMM), F=214.81, P<0.01, n=208; toward: GAMM, F=373.92, P<0.01, n=56]. There were significant effects of initial orientation on the turn angle α in away and toward responses (Figure 3—figure supplement 2; away: GAMM, F=90.88, P<0.01, n=208; toward: GAMM, F=42.48, P<0.01, n=56). In the overall frequency distribution of ETs pooling the data on all initial orientations and both toward and away responses, there were two large peaks at 120–130° and 170–180°, and one small peak at around −80° (Figure 3C). These 3 peaks were confirmed by the Gaussian mixture model analysis [29], where we fitted 1–9 Gaussian curves to the ETs, and selected the most parsimonious model based on the Akaike Information Criterion (AIC) (Figure 3—source data 1).

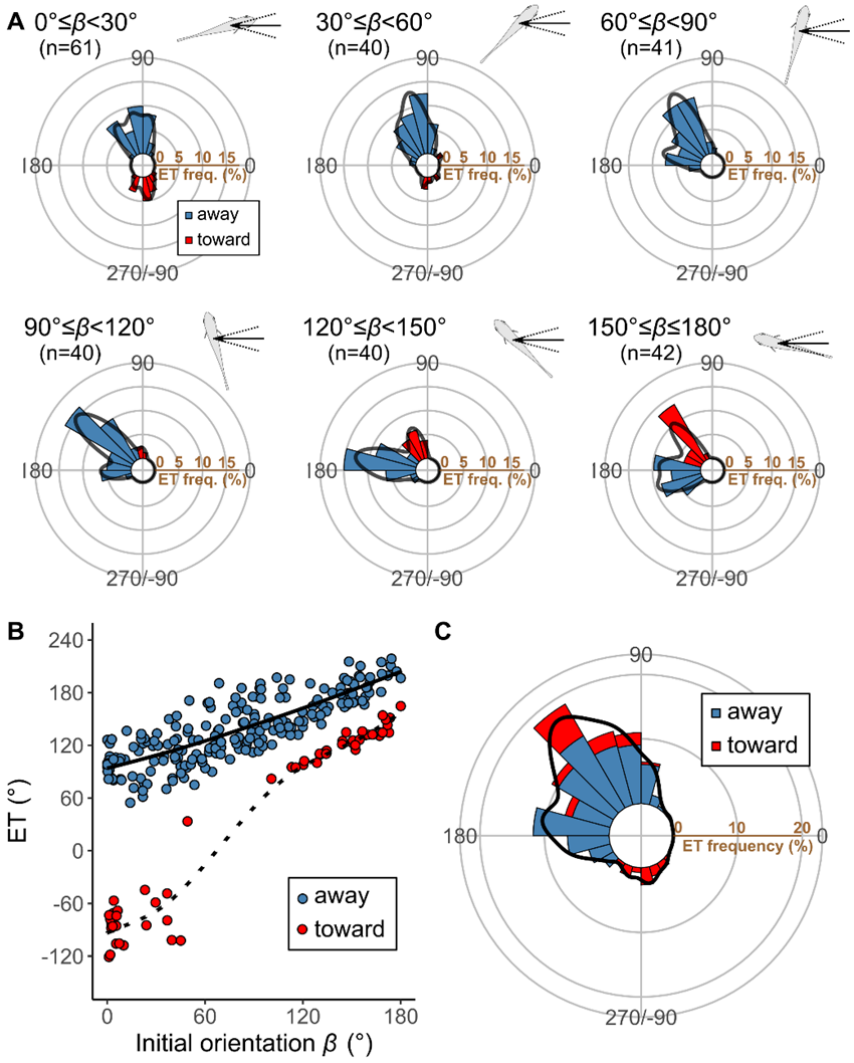

Figure 3. Results of the experiments of *Pagrus major* attacked by a dummy predator (i.e., a cast of *Sebastiscus marmoratus*). (A) Circular histograms of escape trajectories (ETs) in 30° initial orientation β bins. Solid lines are estimated by the kernel probability density function. Concentric circles represent 5% of the total sample sizes within each β bin, the bin intervals are 15°, and the bandwidths of the kernel are 50. A drawing of the prey and predator's approach direction is shown in the upper right corner of each graph. The arrow and dotted lines represent the median value and range of predator's approach direction, respectively. (B) Relationship between initial orientation and ET. Different colors represent the away (blue) and toward (red) responses. Solid and dotted lines are estimated by the generalized additive mixed model (GAMM). (C) Circular histogram of ETs pooling all the data shown in A. Solid lines are estimated by the kernel probability density function. Concentric circles represent 10% of the total sample sizes, the bin intervals are 15°, and the bandwidths of the kernel are 50. The predator's approach direction is represented by 0°. The dataset and R code are available at Figshare ("Dataset1.csv" and "Source code 1.R") [n=264 (208 away and 56 toward responses) from 23 individuals].

Figure supplement 1. Representatives of the kinematics of the prey and the predator over time.

Figure supplement 2. Relationship between initial orientation β and turn angle α in the experiment.

Figure supplement 3. Sketch of the experimental apparatus.

Source data 1. Akaike information criterion for 1–9 Gaussian mixture models to estimate the ET distribution.

There were no significant effects of predator speed on the ET and $|\alpha|$ in either the toward or the away responses (ET, away: GAMM, F=0.01, P=0.93, n=208; ET, toward: GAMM, F=0.05, P=0.82, n=56; $|\alpha|$, away: GAMM, F=0.01, P=0.93, n=208; $|\alpha|$, toward: GAMM, F=0.05, P=0.82, n=56). There were no significant effects of predator speed [slow (from the minimum to the 33.3% quantile): 0.13~0.93 m/s; and fast (from the 66.7% quantile to the maximum): 1.29~1.88 m/s] on the variations of ETs and $|\alpha|$ in all 30° initial orientation bins (Levene's test, W=0.02~3.22, P=0.09~0.88, n=22~47).

Determination of Parameter Values. To predict the relationship between the ET ($\alpha+\beta$) and the relative time difference T_{diff} in each initial orientation (β) by the geometric model, we needed D_{width}, R_{device}, D_1, U_{prey}, $T_1(|\alpha|)$, D_{attack}, and U_{pred}. The methods for determining parameter values are summarized in Table 1. D_{width} and R_{device} were determined from the mouth shape of the predator (the sacrificed specimen for making the dummy predator) when fully opened, which were 18 and 199 mm, respectively. D_1, U_{prey}, and $T_1(|\alpha|)$ were directly estimated by analyzing the escape responses of the prey. Because we have no previous knowledge about the values of U_{pred} and D_{attack} that the prey regards as dangerous, optimal values of U_{pred} and D_{attack} were determined iteratively by comparing model outputs with observed ETs. These optimal values were checked afterward with the data from previously published predator-prey experiments on the same species of prey and predator [12]. We applied this optimization procedure to estimating U_{pred} instead of measuring the dummy predator speed per trial in the experiment because there was no significant effect of predator speed on ET in the experiment, suggesting that the prey is likely to have optimized their ETs based on a fixed predator speed (See Discussion for details). This assumption was also supported by the follow-up analysis using the dummy predator speed per trial, where the model fits became worse compared to the model using the fixed predator speed estimated through the optimization procedure (Table 3—source data 1; Figure 5—figure supplement 1).

The distance of the fast-start phase (D_1) was regarded as 15 mm based on the relationship between displacement and velocity of the prey in the experiments (Figure 4—figure supplement 1), where the velocity increased up to about 15 mm of displacement from the initial position, beyond which it plateaus; over the 15 mm displacement from the initial position, there were no significant differences in the mean velocity between any combinations of 3-mm intervals in any 30° $|\alpha|$ bins

(Figure 4—figure supplement 1; paired *t*-test with Bonferroni's correction, all P=1.00, n=23). There were significant effects of $|\alpha|$ on the time for a displacement of 15 mm from the initial position (GAMM, F=78.84, P<0.01, n=263; note that the sample size is smaller than the total number of observations, 264, because the prey did not move over 15 mm in one case) and on the mean velocity during the displacement (GAMM, F=76.00, P<0.01, n=263). However, there were no significant effects of $|\alpha|$ on the time required for a displacement of 15 to 30 mm from the initial position (GAMM, F=1.52, P=0.22, n=257; note that the sample size is smaller than the total number of observations, 264, because the prey did not move over 30 mm in 7 cases) and on the mean velocity during the displacement (GAMM, F=0.89, P=0.27, n=257). Therefore, the time required for the prey to turn was incorporated into the model by analyzing the relationship between $|\alpha|$ and the time required for a displacement of 15 mm. The mean velocity of the prey during the constant phase U_{prey} was estimated to be 1.04 m s^{-1}, based on the experimental data. Because the cut-off distance might affect the overall results of the study, we have repeated all the statistical analyses (See Tables 2, 3, and the text below for results with a cut-off distance of 15 mm) with cut-off distances of 10 and 20 mm and confirmed that the overall results are insensitive to the changes (Table 2—source data 1; Table 3—source data 2).

Table 1. Methods for determining parameter values

Symbol	Description	Value	Method
D_{width}	the half-width of the predator capture device (e.g., mouth)	18 mm	measured directly from the dummy predator (a sacrificed individual)
R_{device}	the radius of the predator's capture device at the moment of attack, which is approximated as an arc	199 mm	measured directly from the dummy predator (a sacrificed individual)
D_1	the displacement from the initial position of prey where it was assumed to end the fast-start phase	15 mm	estimated from the escape kinematics of prey in the experiment
U_{prey}	the prey speed after the displacement of D_1, which is assumed to be constant	1.04 m s^{-1}	estimated from the escape kinematics of prey in the experiment
$T_1(\|\alpha\|)$	the time required for a displacement of D_1 from the initial position of the prey, given by a function of turn angle $\|\alpha\|$	Figure 4A	estimated from the escape kinematics of prey in the experiment
D_{attack}	the distance between the prey's initial position and the tip of the predator capture device at the end of the predator attack	35 mm	optimized by comparing the model outputs with experimental data
U_{pred}	the predator speed, which is assumed to be constant	1.54 m s^{-1}	optimized by comparing the model outputs with experimental data

The relationship between $|\alpha|$ and the time required for a displacement of 15 mm, $T_1(|\alpha|)$, is shown in Figure 4. The time was constant up to 44° of $|\alpha|$, above which the time linearly increased in response to the increase of $|\alpha|$ (Figure 4A). In the hierarchical Bayesian model, the lowest widely applicable or Watanabe-Akaike information criterion (WAIC) was obtained for the piecewise linear regression model (Table 2). To understand the possible mechanism of the relationship, the relationship between $|\alpha|$ and initial velocity after a stage 1 turn, calculated as the displacement per second during the 10 milliseconds (ms) after the turn, was also evaluated (Figure 4B). The velocity increased in response to $|\alpha|$ up to 46°, beyond which it plateaus. In the hierarchical Bayesian model, the lowest WAIC was obtained for the piecewise linear regression model (Table 2). In both relationships, the regression lines by the piecewise linear model were similar to those by the GAMM, suggesting that the general trends of the relationships were clearly captured by this method. The change points of the two relationships were not significantly different [difference: 1.70±18.01° (mean±95% Bayesian credible intervals)]. These results indicate that fish with a small $|\alpha|$ (<<45°) can accomplish the stage 1 turn quickly but their velocity after the turn is lower, while fish with an intermediate $|\alpha|$ (=45°) spend a longer time on the stage 1 turn, but their velocity after the turn is higher. Fish with a large $|\alpha|$ (>> 45°) spend a still longer time on the stage 1 turn, but their velocity after the turn is similar to that with an intermediate $|\alpha|$ (Figure 4).

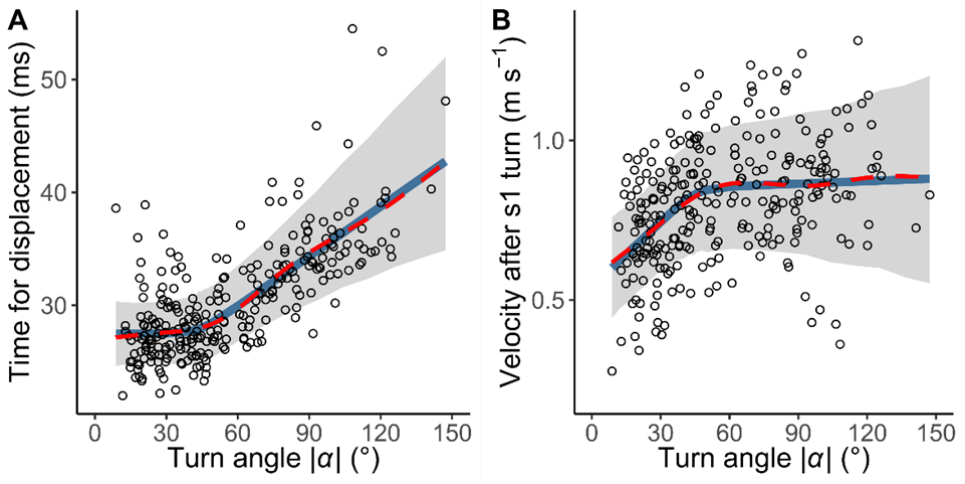

Figure 4. The relationship between the absolute value of the turn angle $|\alpha|$ and time-distance variables. (A) Relationship between $|\alpha|$ and the time required for a displacement of 15 mm from the initial position of the prey (n=263 from 23 individuals). (B) Relationship between $|\alpha|$ and the initial velocity after stage 1 turn (n=264 from 23 individuals). Solid blue lines are estimated by the piecewise linear regression model, and red dashed lines are estimated by the generalized additive mixed model (GAMM). The shaded regions indicate the 95% Bayesian

credible intervals of the piecewise linear regression model. The dataset and R code are available at Figshare ("Source code 1.R", "Source code 2.pdf", "Source code 3.pdf", and "Dataset1.csv").

Figure supplement 1. Relationship between displacement from the initial position and mean velocity during the displacement for each turn angle ($|\alpha|$) bin.

We have optimized the values of U_{pred} and D_{attack} from the perspective of the prey using the experimental data (See Materials and Methods for details). Briefly, the optimal values for prey were obtained using the ranking index, where 0 means that the real fish chose the theoretically optimal ET where T_{diff} is the maximum, and 1 means that the real fish chose the theoretically worst ET where T_{diff} is the minimum (e.g., going toward the predator). The result shows that the optimal value of D_{attack} is 34.73 mm and the optimal value of U_{pred} is 1.54 m s^{-1}. Using data from previously published predator-prey experiments on the same species of prey and predator [12], we show that the estimated D_{attack} value is at the upper limit of the empirical data and the estimated U_{pred} value is higher than the mean of the observed predator speed (Figure 5—figure supplement 2A and B). Similarly, the estimated U_{pred} value is higher than the mean of the observed dummy predator speed in our experiment (Figure 5—figure supplement 2C and D). These results suggest that the values independently estimated in the present study are reasonable, and the prey may choose ETs by overestimating the values of D_{attack} and U_{pred}.

Table 2. Widely applicable or Watanabe–Akaike information criterion (WAIC) for each model in the hierarchical Bayesian models (n=263 and 264, respectively, from 23 individuals). The dataset and R code are available at Figshare ("Dataset1.csv", "Source code 2.pdf", and "Source code 3.pdf").

Relationship	WAIC	ΔWAIC
$\|\alpha\|$–T_1 relationship		
Piecewise linear	1363.7	0
Linear	1376.7	7.0
Constant	1581.1	217.4
$\|\alpha\|$–initial velocity after stage 1 turn relationship		
Piecewise linear	–218.1	0
Linear	–205.1	13.0
Constant	–171.5	46.6

$|\alpha|$, absolute value of the turn angle; T_1, time required for a displacement of 15 mm from the initial position. The best models are shown in bold.

Source data 1. The case where the distance for the fast-start phase was regarded as either 10 or 20 mm.

Comparison of Model Predictions and Experimental Data. Figure 5A plots the relationships between the ET and the relative time difference T_{diff} for different initial orientations β, estimated by the geometric model; Figure 5B plots the relationship between the initial orientation and the theoretical ET. Forty-one percent, 76%, and 94% of observed ETs were within the top 10%, 25%, and 40% quantiles, respectively (0.1, 0.25, 0.40 ranking index) of the theoretical ETs (Figure 5B and Figure 5—figure supplement 3). In general, the predicted ETs are in line with the observed ones, where the model predicts a multimodal pattern of ET with a higher peak (i.e., optimal ET) at the maximum T_{diff} ($T_{diff,1}$) and a second lower peak (i.e., suboptimal ET) at the second local maximum of T_{diff} ($T_{diff,2}$). When the initial orientation is <20° (Figures 5A; β =15°, 5B and 6B), the optimal and suboptimal ETs are around 100° (away response) and −100° (toward response), respectively, which is consistent with the bimodal distribution of our experiment (Figure 3A; $0° \leq \beta < 30°$). At initial orientations in the range 20–60°, the suboptimal ET switches from around −100° to 170° (Figures 5A; β =45°, 5B and 6B), although $T_{diff,2}$ is extremely small compared to $T_{diff,1}$ (Figures 5A; β =45°, 5B and 6B). Accordingly, the second peak (i.e., at around 170°) was negligible in our experimental data (Figure 3A; $30° \leq \beta < 60°$), even though the fish can potentially reach such an ET (i.e., from such an initial orientation, an 170° ET is within the upper limit of $|\alpha|$, 147°). When the initial orientation is 60–120° (Figures 5A; β =75° and β =105°, 5B and 6B), the optimal ET is 100–140° (gradually shifting from 100° to 140°), and the suboptimal ET is around 170°. These two peaks and the shift of the optimal ET are consistent with the experimental results (Figure 3A; $60° \leq \beta < 90°$ and $90° \leq \beta < 120°$). The values of the optimal and suboptimal ETs are reversed at initial orientations >120° (Figures 5B and 6B), as the optimal and suboptimal values become 170–180° and around 140°, respectively (Figure 5A). These results are again consistent with the bimodal distribution of our experiments (Figure 3A; $120° \leq \beta < 150°$ and $150° \leq \beta \leq 180°$).

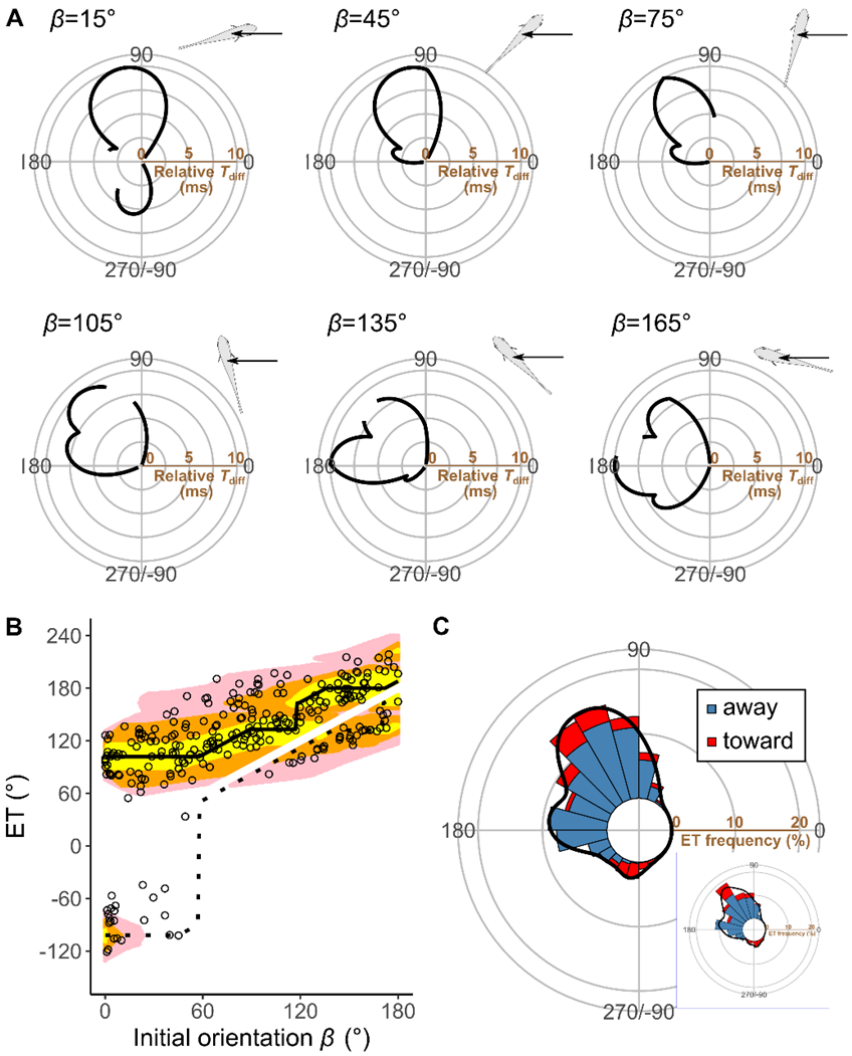

Figure 5. Model estimates. (A) Relationship between the escape trajectory (ET) and the time difference between the prey and predator T_{diff} in different initial orientations β. The time difference of the best ET was regarded as 10 ms, and the relative time differences between 0 and 10 ms are shown by solid lines. Areas without solid lines indicate that either the time difference is below 0 or the fish cannot reach that ET because of the constraint on the possible range of turn angles $|\alpha|$. A drawing of prey and predator's approach direction (arrow) is shown in the upper right corner of each graph. (B) Relationship between the initial orientation β and ET. Solid and dotted lines represent the best-estimated away and toward responses, respectively. Different colors represent the top 10%, 25%, and 40% quantiles of the time difference between the prey and predator within all possible ETs. (C) Circular histogram of the theoretical ETs, estimated by a Monte Carlo simulation. The probability of selection of an ET was determined by the truncated normal distribution of the optimal ranking index (Figure 5—figure supplement 3). This process was repeated 1000 times to estimate the frequency distribution of the theoretical ETs. Colors in the bars represent the away (blue) or toward (red) responses. Black lines represent the kernel probability density function. Concentric circles represent 10 % of the total sample sizes, the bin intervals are 15°, and the bandwidths of the kernel are 50. Circular histogram of the observed ETs (Figure 3C) is shown in the lower right panel for comparison. The predator's approach direction is represented by 0°. The dataset and R code are available at Figshare

("Dataset1.csv" and "Source code 1.R") (n=264 from 23 individuals for experimental data, and n=264000 for Monte Carlo simulation).

Figure supplement 1. Estimates of the model using actual predator speed per trial in the experiment.

Figure supplement 2. Predator *Sebastiscus marmoratus* attack parameters.

Figure supplement 3. Histogram of the ranking index.

Figure supplement 4. Estimates of the model with D_{attack} and without $T_1(|\alpha|)$.

Figure supplement 5. Estimates of the model with $T_1(|\alpha|)$ and without D_{attack}.

Figure supplement 6. Estimates of the model that includes neither D_{attack} nor $T_1(|\alpha|)$.

Figure 5C shows the circular histogram of the overall theoretical ETs estimated by Monte Carlo simulation. The theoretical ETs show two large peaks at around 110–130° and 170–180°, and one small peak at around −100° (Figure 5C). This theoretically estimated ET distribution is similar to the frequency distribution of the observed ETs (Figure 3C); there were no significant differences in the frequency distribution between theoretical ETs (n=264 per simulation) and observed ETs (n=264) in 971 of 1000 simulations (Table 3; two-sample Kuiper test, median V=0.11, median P=0.44).

Table 3. Comparison of the distribution of escape trajectories (ETs) between the model prediction (n=264 per simulation ×1000 times) and experimental data (n=264) using the two-sample Kuiper test. The dataset and R code are available at Figshare ("Dataset1.csv" and "Source code 1.R").

Model	Median Kuiper's V	Median P	Rate of $P > 0.05$
With both D_{attack} and $T_1(\|\alpha\|)$	0.11	0.44	0.97
With D_{attack} and without $T_1(\|\alpha\|)$	0.26	< 0.01	0.00
Without D_{attack} and with $T_1(\|\alpha\|)$	0.18	< 0.01	0.12
Neither D_{attack} nor $T_1(\|\alpha\|)$	0.28	< 0.01	0.00

D_{attack}, distance between the prey's initial position and the endpoint of the predator attack; $T_1(|\alpha|)$, relationship between the absolute value of the turn angle and the time required for a 15-mm displacement from the initial position (i.e., the time required for the prey to turn).

Source data 1. The case where U_{pred} was determined from the dummy predator speed per trial in the experiment.

Source data 2. The case where the distance for the fast-start phase was regarded as either 10 or 20 mm.

To investigate how the initial orientation of the prey modulates the proportion of using the theoretically optimal ET (i.e., where T_{diff} is the maximum, $T_{diff,1}$) compared to using the suboptimal ET (i.e., where T_{diff} is the second local maximum, $T_{diff,2}$), we calculated the optimal ET advantage ($T_{diff,1}-T_{diff,2}$) (Figure 6A), which represents the difference in the buffer time available for the prey to escape from the predator, at different initial orientations. The fish chose the optimal and suboptimal ETs to a similar extent when the optimal ET advantage is negligible (Figure 6C). For example, when

looking at the optimal ET advantage <2 ms, where the initial orientation is 0–7° and 106–180° (46% of all initial orientations), the proportion of the optimal ET used was only 55% (Figure 6B and C). On the other hand, the proportion of the optimal ET used was 81% when the optimal ET advantage is higher than 6 ms (i.e., when the initial orientation is 21–75°) (Figure 6B and C). There was a significant effect of optimal ET advantage on the proportion of the optimal ET used by fish tested in our experiments (Mixed-effects logistic regression analysis, χ^2 =10.72, P<0.01, n=247).

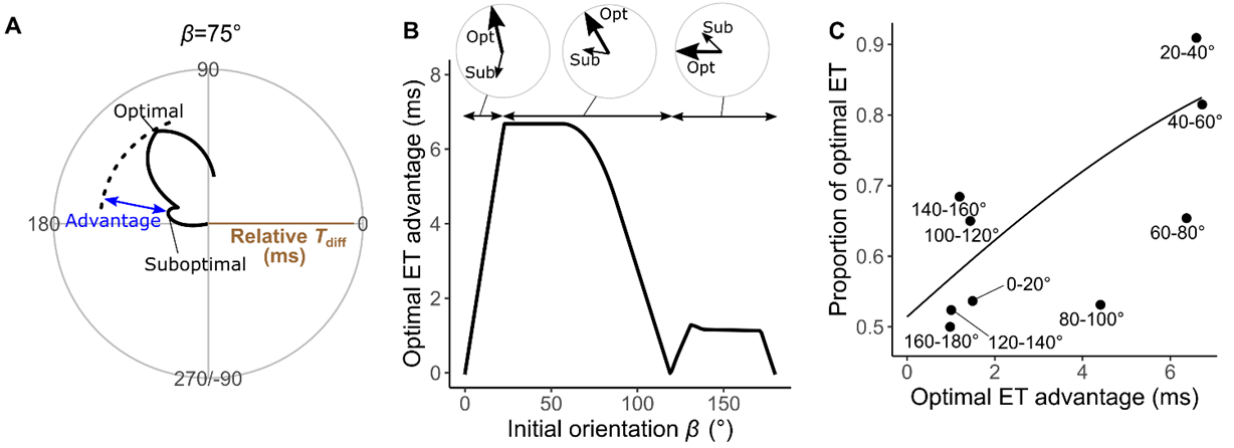

Figure 6. Analyses of the probability that the prey chooses the optimal vs. suboptimal ETs. (A) The time difference between the prey and predator T_{diff} at the initial orientation β of 75° is shown as an example. We defined the difference between the maximum of T_{diff} (at the optimal ET) and the second local maximum of T_{diff} (at the suboptimal ET) as the optimal ET advantage. (B) Relationship between the initial orientation β and the optimal ET advantage. Large and small arrows in circles represent the optimal and suboptimal ETs, respectively, for each β sectors. (C) Relationship between the optimal ET advantage and the proportion of the optimal ET used by the real prey in 20° initial orientation β bins. The line was estimated by the mixed effects logistic regression analysis. The dataset and R code are available at Figshare ("Dataset1.csv" and "Source code 1.R") (n=247 from 23 individuals).

To investigate the effects of two factors [i.e., the endpoint of the predator attack D_{attack} and the time required for the prey to turn $T_1(|\alpha|)$] on the predictions of ET separately, we constructed three additional geometric models (Figure 5—figure supplement 4–6): a model that includes only D_{attack}, a model that includes only $T_1(|\alpha|)$, and a null model that includes neither factors (Figure 2A and [15]). In all of these models, the theoretical ET distributions estimated through Monte Carlo simulations were significantly different from the observed ET distributions (Table 3; two-sample Kuiper test, median $P<0.01$). Although the model with D_{attack} and the model with $T_1(|\alpha|)$ show multimodal patterns of ET distribution, the simulation based on these models do not match the experimental data, likely because of differences in the values and relative heights of the peaks (Figure 5—figure supplement 4 and 5). The null model shows a unimodal pattern of ET distribution (Figure 5—figure supplement 6).

Potential application of the model to other ET patterns. Although many fish species and animals from other taxa exhibit multiple preferred ETs similar to what we observed here, some animals show different patterns of ETs: e.g., a single preferred ET either at around 180° [48] or at around 90° [27], and multiple preferred ETs at small and large angles from the predator's approach direction [49-51] (Figure 7A–C). To investigate whether our geometric model has the potential to explain these different ET patterns, we changed the values of model parameters (e.g., U_{pred}, D_{attack}) within a realistic range, and explored whether such adjustments can produce the ET patterns observed in the original work. At small U_{pred}, the model predicts one strong peak at around 180° (Figure 7D), whereas at large U_{pred}, the model predicts a strong peak at around 90° (Figure 7E). The model where the predator can adjust the approach path and its attack lasts for a long distance (i.e., large D_{attack}) predicts multiple preferred ETs directed at small (at around 30°) and large (at around 170°) angles from the predator's approach direction (Figure 7F). These results indicate that our model has the potential to explain various patterns of observed animal escape trajectories. See Figure 7—figure supplement 1–9 for details of the effect of each parameter on the ET distribution.

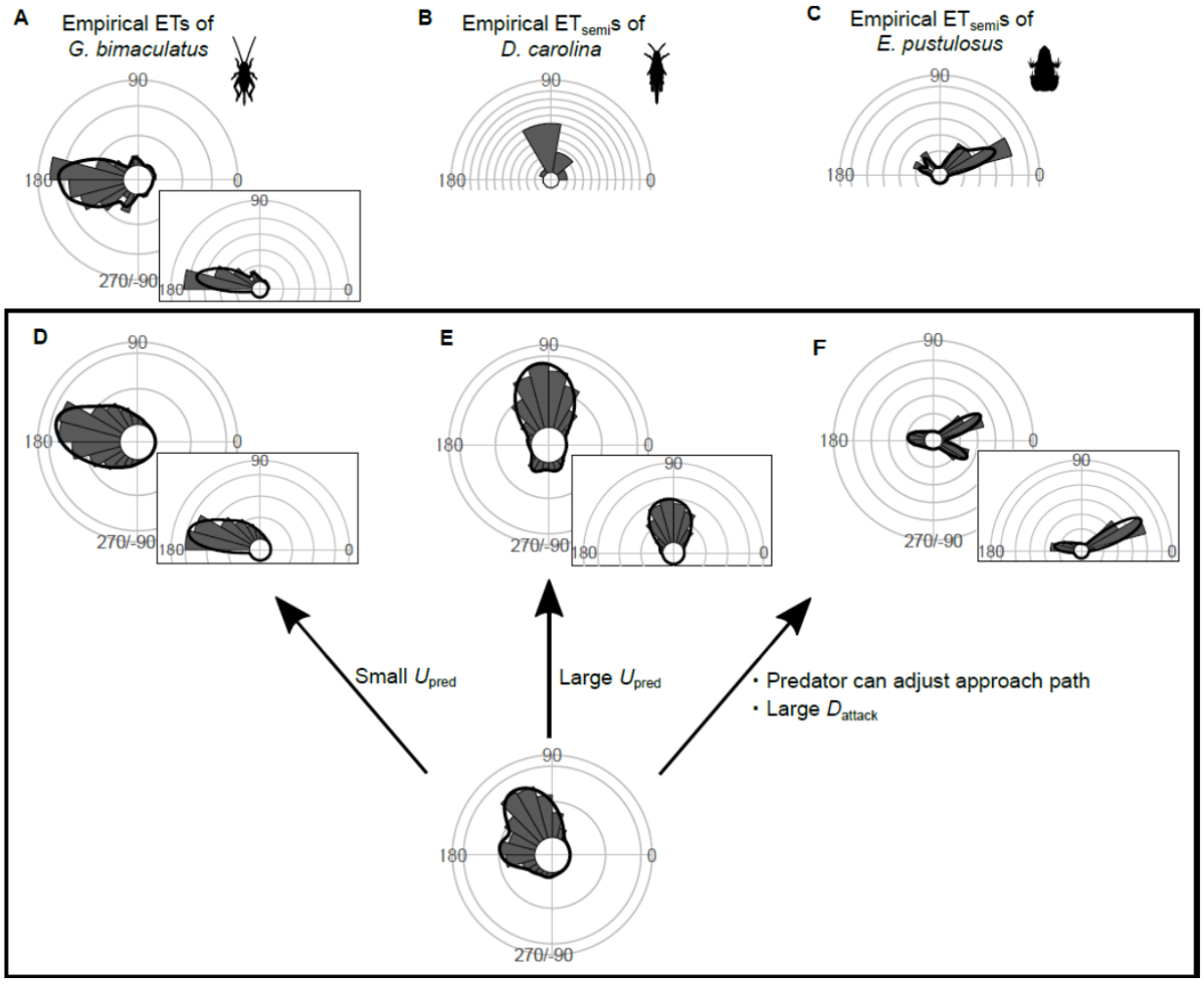

Figure 7. Circular histograms of other typical empirical ET distribution patterns and the potential explanations by the geometric model. Some previous studies have used the different definition for calculating the angles for escape trajectories, in which the values range from 0° (directly toward the threat) to 180° (opposite to the threat), thereby using only one semicircle regardless of their turning direction and magnitude (e.g., both 120° and 240° of ETs are regarded as 120°). This angle is denoted as ET_{semi}, and is shown by a semicircular plot. (A) Unimodal ET distribution pattern at around 180° in two-spotted cricket *Gryllus bimaculatus* escaping from the air-puff stimulus. Data were obtained from Figure 4 in Kanou et al. (1999) [48]. (B) Unimodal ET_{semi} distribution pattern at around 90° in Carolina grasshopper *Dissosteira carolina* escaping from an approaching human. Data were obtained from Figure 3 in Cooper (2006) [27]. (C) Bimodal ET_{semi} distribution pattern directed at small and large angles from the predator's approach direction in túngara frog *Engystomops pustulosus* escaping from an approaching dummy bat. Data were obtained from Figure 5b in Bulbert et al. (2015) [51]. (D) Unimodal ET distribution pattern at around 180°, estimated by a Monte Carlo simulation of the geometric model. In this case, the predator speed U_{pred} is very small (i.e., $K=U_{pred}/U_{prey}=0.3$), and the other parameter values are the same as the values used to explain the escape response of *Pagrus major*. (E) Unimodal ET distribution pattern at around 90°, estimated by a Monte Carlo simulation of the model. In this case, U_{pred} is very large (i.e., $K=U_{pred}/U_{prey}=7.5$), and the other parameter values are the same as the values used to explain the escape response of *P. major*. (F) Bimodal ET distribution pattern directed at small and large angles from the predator's approach direction, estimated by a Monte Carlo simulation of the

geometric model where the predator can adjust its approach path. In this case, $D_{initial}$ is 130 mm, D_{react} is 70 mm, R_{turn} is 12 mm, D_{attack} is 400 mm, SD_{choice} is 0.23, and the other parameter values are the same as the values used for explaining the escape response of *P. major*. Black lines represent the kernel probability density function with a bandwidth of 50, and concentric circles represent 10 % of the total sample sizes. See Table 1 and the text for details of the definitions of the variables. The R code is available at Figshare ("Source code 1.R").

Figure supplement 1. Effect of U_{pred} on the theoretical ET and ET_{semi} distributions.

Figure supplement 2. Effect of D_{attack} on the theoretical ET and ET_{semi} distributions.

Figure supplement 3. Effect of R_{device} on the theoretical ET and ET_{semi} distributions.

Figure supplement 4. Effect of SD_{choice} on the theoretical ET and ET_{semi} distributions.

Figure supplement 5. Effect of U_{pred} on the theoretical ET and ET_{semi} distributions, where the predator can adjust its approach path.

Figure supplement 6. Effect of D_{attack} on the theoretical ET and ET_{semi} distributions, where the predator can adjust its approach path.

Figure supplement 7. Effect of $D_{initial}$ on the theoretical ET and ET_{semi} distributions, where the predator can adjust its approach path.

Figure supplement 8. Effect of R_{turn} on the theoretical ET and ET_{semi} distributions, where the predator can adjust its approach path.

Figure supplement 9. Effect of SD_{choice} on the theoretical ET and ET_{semi} distributions, where the predator can adjust its approach path.

Discussion

Our geometric model, incorporating the endpoint of the predator attack, D_{attack}, and the time required for the prey to turn, $T_1(|\alpha|)$, to maximize the difference between the prey and the predator in the time of arrival at the edge of the safety zone, T_{diff}, clearly explains the multimodal patterns of ETs in *P. major*. Figure 8 shows an example of how multiple ETs result in successful escapes from predators. Specifically, according to the model, when the prey escapes at 140° or 170°, it will not be captured by the predator. On the other hand, when the prey escapes along an intermediate trajectory (157°), it will be captured because it swims toward the corner of the danger zone to exit it, and therefore it needs to travel a longer distance than when escaping at 140° or 170°. This example illustrates that the multimodal patterns of ETs are likely to be attributable to the existence of two escape routes: either moving sideways to depart from the predator's strike path or moving opposite to the predator's direction to outrun it. Interestingly, both components of the predator-prey interaction [i.e., D_{attack} and $T_1(|\alpha|)$] added to the previous model [15] are important for accurate predictions of the ET distribution because when they are considered by the model separately, the predictions do not match the experimental data (Figure 5—figure supplement 4 and 5; Table 3).

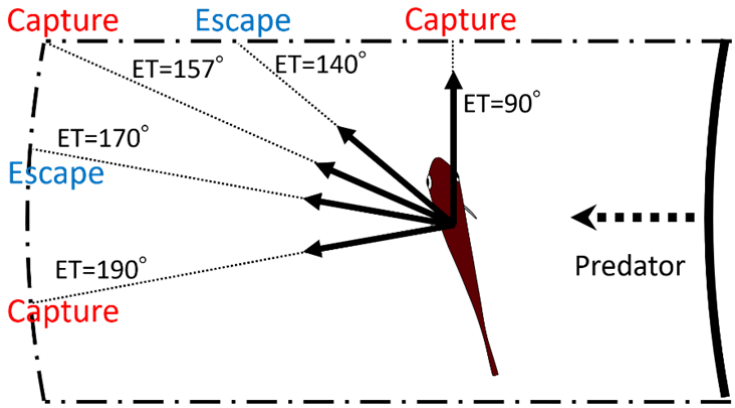

Figure 8. Schematic drawing showing how multiple escape trajectories (ETs) result in successful escapes from predators. The area enclosed by dash-dotted lines represents the danger zone the prey needs to exit in order to escape predation, outside of which is the safety zone. When the prey escapes toward the corner of the danger zone (ET=157°) to exit it, it needs to travel a relatively long distance and therefore the predator can catch it. On the other hand, when the prey escapes with an ET at 170° or 140°, it covers a shorter distance and can reach the safety zone before the predator's arrival. When the prey escapes with an even smaller ET (90°), it will be captured because the shorter travel distance for the predator overrides the benefits of the smaller turn and shorter travel distance for the prey. When the prey escapes with an even larger ET (190°), it will also be captured, because the prey requires a longer time to turn than if escaping along the 170° ET, whereas the travel distance for both predator and prey is the same as that for the 170° ET. In this example, the initial orientation, flight initiation distance, and the body length posterior to the center of mass were set as 110°, 60 mm and 30 mm, respectively.

Two different escape tactics have been proposed to enhance the success of predator evasion [16, 17]: the optimal tactic, which maximizes T_{diff} (i.e., the distance between the prey and the predator) [4, 14, 15, 18], and the protean tactic, which maximizes unpredictability to prevent predators from adjusting their strike trajectories accordingly [19-22]. Our results suggest that the prey combines these two different tactics by using multiple preferred ETs. Specifically, when the optimal ET advantage is large (i.e., when the initial orientation is 20–60°), the prey mainly uses the optimal ET (Figures 3A and 6). However, when the optimal ET advantage over the suboptimal ET is negligible (i.e., the initial orientation is close to 0° or within the range 110–180°), the prey uses optimal and suboptimal ETs to a similar extent (Figures 3A and 6). In such cases, the escape trajectory of the prey would be highly unpredictable for the predator. The unpredictability at initial orientations near 0° and 180° is consistent with the study that applied the conventional geometric model to the larval zebrafish *Danio rerio* [47], where the optimal and suboptimal ETs are approximately symmetrical to the axis of the predator attack. This phenomenon can be explained by the toward-away indecision at orientations nearly perpendicular to the threat [28, 52]. On the other hand, the unpredictability observed at initial orientations near 110–180° is related to the similarly

advantageous choice between escaping with an ET at around 140° or 180°. Interestingly, at initial orientations >120°, our results show that these two ETs are reached by using toward and away responses, respectively. The overlap between the ETs of toward and away responses in the overall dataset (Figure 3) suggests that toward responses are not "tactical mistakes" of the prey that turns toward a threat, but are simply related to reaching an optimal or suboptimal ET. These results suggest that the prey strategically adjusts the use of optimal and protean tactics based on their initial orientation. This allows the prey to have unpredictable ETs, thereby preventing predators from anticipating their escape behavior, while keeping T_{diff} large enough to enter the safety zone before the predator reaches it.

From a behavioral decision-making perspective, our results suggest that the prey follows the matching law [30-33], where the probability that an optimal or suboptimal ET is chosen is proportional to its chances of survival (i.e., T_{diff}). As the matching law predicts [33], the prey stochastically draws from a Bernoulli distribution dictated by the optimal ET advantage for the binary choice between an optimal or suboptimal ET, thereby introducing an element of unpredictability, which can prevent predators from learning. Because most empirical studies supporting the matching law use unnatural reinforcement learning paradigms or human behaviors [30-33], this result suggests that the matching law is also applicable to animal behavior in realistic contexts. Further research using a real predator and dummy prey (e.g., [53]) controlled to escape toward an optimal or suboptimal ET with various specific probabilities is required to test whether our model accurately predicts the best combination of the optimal and suboptimal ETs when accounting for the predator learning.

A relevant question from a perspective of neurosensory physiology is how the animals are able to determine their ETs within milliseconds of response time. The initial orientation of the prey has been incorporated into various neural circuit models [54-57], but these models assume that prey animals always escape in a 180° direction (i.e., opposite to the stimulus source), irrespective of the initial orientation. However, the present study shows that animals use suboptimal ETs as well as optimal ETs, and that these ETs may change in a nonlinear fashion, depending on the initial orientation. More specifically, the Mauthner cell and other neurons involved may be activated in accordance with the Bernoulli probabilities dictated by the model, which determine the proportions of away and toward responses and the magnitude of turn to achieve the multiple preferred ETs. Thus, we require new neurophysiological models of ETs to understand how neural circuits process the

sensory cues of a threatening stimulus, resulting in muscle actions that generate multiple preferred ETs.

Our geometric model assumes that the prey determines the ETs based on a fixed predator speed. This assumption is supported by the results of our experiments, where the effects of predator speed on the mean and variability of ETs are not significant. Although we did not find any effect of predator speed, it is possible that a speed outside the range we used may affect ETs. Recent studies show that larval zebrafish exhibit less variable ETs under faster threats than they do under slower threats [58, 59], and the difference in ET variability between fast and slow threats is dependent on whether the Mauthner cell is active or not [59]. Therefore, any differences in the ET variability of the present study compared to previous studies could be related to the different involvement of the Mauthner-cells. Using the conventional geometric model, Soto *et al.* [14] showed that the choice of ET only matters to a prey when the predator speed is intermediate, because a prey that is much faster than its predator can escape by a broad range of ETs, whereas a prey that is much slower than its predator cannot escape by any ETs [18]. The predator speed used in this study is in the range of the real predator speed in the previous study using the same species of both predator and prey [12]. Thus, our results are ecologically relevant, and the prey is likely to have optimized their ETs based on a fixed predator speed, where the choice of ET strongly affects their survival.

The relationship between $|\alpha|$ and the time required for a 15-mm displacement, $T_1(|\alpha|)$, (Figure 4A) indicates that the time required for a 15-mm displacement is relatively constant up to an $|\alpha|$ of about 45°, while a further change in $|\alpha|$ requires additional time. This relationship is likely to be attributable to the kinematics and hydrodynamics of the C-start escape response, because the initial velocity after the stage 1 turn increases linearly up to about 45°, beyond which it plateaus (Figure 4B). Interestingly, a recent study on swimming efficiency during acceleration found that efficiency increases linearly with yaw amplitudes up to a certain value, beyond which efficiency plateaus [60].

Based on the STRANGE framework for animal behavior research [61], we identified potential biases that may limit the generalizability of our findings. Our empirical data are obtained from one species of hatchery-reared fish with a specific life stage, which has never experienced predators. Therefore, this study alone cannot exclude the possibility that fish of different species, origins, life stages, and rearing histories have different rules for ETs, which our model cannot explain. However, similar multiple preferred ETs have been observed in many fish species and other animal taxa, including hatcheries/wild origins and different life stages [26]. Therefore, we believe that our

model is not specific to our experiment but is applicable to other cases showing multiple preferred ETs.

We show that our model has the potential to explain other empirically observed ET patterns (Figure 7). Based on the model assuming that the predator makes an in-line attack toward the prey, which is realistic for ambush and stalk-and-attack predators [62] (e.g., frogs [11], spiders [13], and fish [12, 35, 36, 63]), either single or multiple ETs at around 90–150° and around 180° are predicted, as have been observed in many empirical studies of animals escaping from ambush predators and artificial stimuli [26]. Based on the model assuming that the predator can adjust its approach path, which is realistic for pursuit predators, multiple ETs directed at small and large angles from the predator's approach direction can be predicted, as observed in the empirical studies of prey escaping from pursuit predators [24, 51]. Further research measuring the escape response in various species and applying the data to our geometric model is required to verify the applicability of our geometric model to various predator-prey systems.

Our work represents a major advancement in understanding the basis of the variability in ETs observed in previous works (reviewed in [26]). Our results suggest that prey use multiple preferred ETs to maximize the time difference between themselves and the attacking predator, while keeping a high level of unpredictability. The results also suggest that prey strategically adjust the use of protean and optimal tactics with respect to the advantage of the optimal ET over the suboptimal ET. Because multimodal ETs similar to what we observed here have been found in many fish species and other animal taxa [26], this behavioral phenotype may result from convergent evolution in phylogenetically distant animals. From a neurosensory perspective, our findings open new avenues to investigate how the animals determine their ETs from multiple options with specific probabilities, which are modulated by the initial orientation with respect to the threat.

Materials and Methods

Definition of the Angles. The C-start escape response consists of an initial bend (stage 1), followed by a return tail flip (stage 2), and continuous swimming or coasting (stage 3) [44, 45]. In line with previous studies [26, 47, 64], we defined initial orientation β, directionality (away or toward responses), turn angle α, and ET $\alpha+\beta$ as follows (Figure 2—figure supplement 1). *Initial orientation* (β): the angle between the line passing through the prey's center of mass (CoM; located at 34% of the total length from the tip of the snout [12]) and the tip of the snout at the onset of stage 1, and the

midline of the predator model attacking in a straight line. Initial orientation ranges from 0° (i.e., when the prey is attacked from front) to 180° (i.e., when the prey is attacked from behind). *Directionality*: the away and toward responses were defined by the first detectable movement of the fish in a direction either away from or toward the predator, respectively [26]. In rare cases (n=3; 1.1% of the total observations) where the initial orientation is exactly 0° (n=1) or 180° (n=2), the counterclockwise and clockwise turns were regarded as away and toward responses, respectively. *Turn angle* (α): the angle between the line passing through the CoM and the tip of the snout at the onset of stage 1, and the line passing through the CoM at the onset of stage 1 and the CoM at the end of stage 2. The angles of the away and toward responses are assigned positive and negative values, respectively. *ET* ($\alpha+\beta$): the angular sum of the initial orientation (β) and the turn angle (α). Because the experimental data exhibited no asymmetry in directionality (Fisher's exact test, P=1.00, n=264) and ET distribution (two-sample Kuiper test, V=0.14, P=0.61, n=264), we pooled the ETs from the left and right sides, treating all fish as though they were attacked from the right side [26]. ET is a circular variable with a cycle of 360°. As the range of $|\beta|$ is 0~180° and the range of $|\alpha|$ was 9~147° in the experiment, the ET value can potentially range from −147° to 327°. Circular graphs are shown with angles from 0 to 360° [65], where negative values such as −90° correspond to positive values shifted by one cycle (in this case, −90°+360°=270°).

Experiment.

Following the STRANGE framework for animal behavior research [61], we provide details of the test samples and experimental procedure in the following two subsections.

Sample Fish: We used young-of-year juvenile hatchery-reared red sea bream *P. major* for the experiment. Sixty-five individuals were purchased from commercial hatcheries (Marua Suisan Co., Ltd., Ehime, Japan), where they were reared communally in artificial tanks. After arriving at the laboratory at Nagasaki University, they were kept in a 200 l polycarbonate tank and were fed with commercial pellets (Otohime C2; Marubeni Nisshin Feed Co. Ltd, Tokyo, Japan) twice a day. The sex of the fish was not determined because the species of this size is in a bisexual juvenile stage [66]. Water temperature was maintained at 23.8 to 24.9℃.

Experimental Procedure: We have elicited the escape response of *P. major* [45.3±3.5 (39.4–51.5)

mm total length, 37.2±2.9 (32.3–42.2) mm standard length, 1.6±0.4 (0.9–2.3) g body weight, mean±s.d. (range), n=23] using a dummy predator. The value of Fulton's condition factor [30.64±2.43 (26.10–35.56), mean±s.d. (range)], calculated by the body weight of the fish divided by the standard length cubed, suggests that all fish were in a good nutritious condition [67, 68]. The experiment was conducted in a plastic tank (540×890×200 mm) filled with seawater to a depth of 80 mm. The water temperature was maintained at 23.8 to 24.7℃. An individual *P. major* was randomly captured by a hand net from the holding tank, introduced into a PVC pipe (60 mm diameter) set in the center of the experimental tank, and acclimated for 15 min. Because it was not difficult to capture any individual by a hand net, there should be no bias in selecting individuals with specific behavioral types. After the acclimation period, the PVC pipe was slowly removed, and the dummy predator, a cast of *Sebastiscus marmoratus* (164 mm in total length and 36 mm in mouth width), was moved toward the *P. major* for a distance of 200 mm (Figure 3—figure supplement 3A). The dummy predator was held in place by a metal pipe anchored to a four-wheel dolly, which is connected to a fixed metal frame via two plastic rubber bands (Figure 3—figure supplement 3B). The wheel dolly was drawn back to provide power for the dummy predator to strike toward the prey. Because the previous work shows that *S. marmoratus* attacks *P. major* using a variable speed [1.10±0.65 (0.09–2.31) m s^{-1}, mean±s.d. (range)] [12], we used various strengths of plastic rubber bands to investigate the effect of predator speed on ET. The fish movements were recorded from above, using a high-speed video camera (HAS-L1; Ditect Co., Tokyo, Japan) at 500 frames s^{-1}. Each individual *P. major* was stimulated from 5 to 23 times with a time interval of at least 15 min, and, in total, 297 trials were conducted. We eliminated 33 trials from the analysis because *P. major* moved away from the striking course of the dummy predator before the stimulation (in 14 trials) and because bubbles obscured the *P. major* image (in 19 trials). The final data analyzed are 5–20 escape responses per individual and, in total, 264 escape responses. The experiments for each *P. major* were accomplished within one day to eliminate possible effects of tank transfer, handling, and change of rearing conditions. The number of recordings of an individual *P. major* was different because we could not allocate the same amount of time to the experiment per day due to the experimental schedule and because the numbers of eliminated data are different among individuals. The recorded videos were analyzed frame by frame using Dipp-Motion Pro 2D (Ditect Co.). The CoM and the tip of the mouth of *P. major* and the tip of the predator's mouth were digitized in each frame to calculate all the kinematic variables. The animal care and experimental procedures were approved by the Animal

Care and Use Committee of the Faculty of Fisheries (Permit No. NF-0002), Nagasaki University in accordance with the Guidelines for Animal Experimentation of the Faculty of Fisheries and the Regulations of the Animal Care and Use Committee, Nagasaki University.

Statistical Analysis: Because our geometric model predicts that the initial orientation β and the predator speed U_{pred} affect the ET and turn angle α, we examined these effects by the experimental data using a GAMM with a normal distribution and identity link function [69]. ET and α were regarded as objective variables, while predator speed and initial orientation were regarded as explanatory variables and were modeled with a B-spline smoother. Fish ID was regarded as a random factor. Smoothed terms were fitted using penalized regression splines, and the amount of smoothing was determined using the restricted maximum likelihood (REML) method. As was done in previous studies [26, 46, 47], the away and toward responses were analyzed separately. The significance of the initial orientation and predator speed was assessed by the *F*-test. The analysis was conducted using R 3.5.3 (R Foundation for Statistical Computing) with the R package *gamm4*.

Determination of Parameter Values.

Determination of the Prey's Kinematic Parameters: The relationship between $|\alpha|$ and the time required for a displacement of 15 mm, $T_1(|\alpha|)$, was estimated by piecewise linear regression [70]. We used piecewise linear regression rather than a commonly used smoothing method such as GAMM, because the smoothing method does not output the timing of the regression change and thus the biological interpretation of the regression curve is problematic [70]. The time required for a displacement of 15 mm was regarded as an objective variable, whereas $|\alpha|$ was regarded as an explanatory variable. Fish ID was included as a covariate in order to take into account potential individual differences in the relationship, $T_1(|\alpha|)$. To detect the possible kinematic mechanism of the relationship $T_1(|\alpha|)$, we also examined the relationship between $|\alpha|$ and initial velocity after the stage 1 turn, using piecewise linear regression. Initial velocity after the stage 1 turn was regarded as an objective variable, $|\alpha|$ was regarded as an explanatory variable, and fish ID was included as a covariate. A hierarchical Bayesian model with a Markov chain Monte Carlo (MCMC) method was used to estimate these relationships [70, 71]. The number of draws per chain, thinning rate, burn-in length, and number of chains were set as 200000, 1, 100000, and 5, respectively. To test the overall fit of the model, the WAIC of the model was compared with those of the null model (constant) and a

simple linear regression model. MCMC was conducted using RStan 2.18.2 (Stan Development Team 2019).

Determination of Predator Speed and Endpoint of the Predator Attack: Because we had no previous knowledge about the values of U_{pred} and D_{attack} that the prey regards as dangerous (i.e., the values of U_{pred} and D_{attack} that trigger a response in the prey), we optimized the values using the experimental data in this study. We have input the obtained values of D_{width}, R_{device}, D_1, U_{prey}, and $T_1(|\alpha|)$ into the theoretical model. The optimal values of U_{pred} and D_{attack} were obtained using the ranking index. The ranks of the observed ETs among the theoretical ET choices of 1° increment were standardized as the ranking index, where 0 means that the real fish chose the theoretically optimal ET where T_{diff} is the maximum, and 1 means that the real fish chose the theoretically worst ET where T_{diff} is the minimum. The optimal set of D_{attack} and U_{pred} values was determined by minimizing the mean ranking index of the observed ETs. The distribution of the optimal ranking index was then fitted to the truncated normal distribution and was used to predict how the fish chose the ETs from the continuum of the theoretically optimal and worst ETs.

Model Predictions. We input the above parameters [D_{width}, R_{device}, D_1, U_{prey}, $T_1(|\alpha|)$, D_{attack}, and U_{pred}] into the model and calculated how the choice of different ETs affects T_{diff} for each initial orientation β. Because there was a constraint on the possible range of $|\alpha|$ (i.e., fish escaping by C-start have a minimum and maximum $|\alpha|$ [40]), the range of $|\alpha|$ was determined based on its minimum and maximum values observed in our experiment, which were 9~147°.

To estimate the overall frequency distribution of ETs that include the data on observed initial orientations, we conducted Monte Carlo simulations. In each observed initial orientation, the ET was chosen from the continuum of the theoretically optimal and worst ETs. The probability of the ET selection was determined by the truncated normal distribution of the optimal ranking index (e.g., the fish could choose theoretically good ETs with higher probability than theoretically bad ETs, but the choice is a continuum based on the truncated normal distribution). This process was repeated 1000 times to robustly estimate the frequency distribution of the theoretical ETs. In each simulation run, the frequency distribution of the theoretical ETs was compared with that of the observed ETs using the two-sample Kuiper test [72].

To investigate how the real prey changes the probability that it uses the theoretically optimal

ET or suboptimal ET, we regarded the difference between the maximum of T_{diff} (at the optimal ET) and the second local maximum of T_{diff} (at the suboptimal ET) as the optimal ET advantage, and theoretically estimated the values for all initial orientations. We then examined the relationship between the optimal ET advantage and the proportion of the optimal ET the prey actually chose using a mixed-effects logistic regression analysis [69]. Each observed ET was designated as the optimal (1) or the suboptimal (0) based on whether the observed ET was closer to the optimal ET or suboptimal ET. When the prey chose the ET that was more than 35° different from both the optimal and suboptimal ETs, the ET data point was removed from the analysis (these cases were rare: 7%). The choice of ET [optimal (1) or suboptimal (0)] was regarded as an objective variable, while the optimal ET advantage was regarded as an explanatory variable. Fish ID was regarded as a random factor. The significance of the optimal ET advantage was assessed by the likelihood ratio test with χ^2 distribution. The analysis was conducted using R 3.5.3 with the R package *lme4*.

To investigate the effects of two factors [i.e., the endpoint of the predator attack D_{attack} and the time required for the prey to turn $T_1(|\alpha|)$] on predictions of ET separately, we compared four geometric models: the model that includes both D_{attack} and $T_1(|\alpha|)$, the model that includes only D_{attack}, the model that includes only $T_1(|\alpha|)$, and the null model. Note that the null model is equivalent to the previous Domenici's model [15]. In all models, the values of U_{pred} and D_{attack} were optimized using the ranking index. The overall frequency distributions of ETs were estimated through Monte Carlo simulations, and in each simulation run, the theoretical ET distribution was compared with the observed ET distribution using the two-sample Kuiper test.

To investigate whether our model has the potential to explain other empirical ET patterns, we changed the values of model parameters (e.g., U_{pred}, D_{attack}) within a realistic range, and conducted Monte Carlo simulations to estimate the frequency distribution of the theoretical ETs. For each initial orientation, ranging from 0° to 180° with an increment of 1°, the ET was chosen based on the probability of the truncated normal distribution (i.e., the continuum of the theoretically optimal and worst ETs), and this process was repeated 100 times. In the model where the predator cannot adjust the strike path (Figure 2B), we fixed three parameters and varied the fourth parameter (U_{pred}, D_{attack}, R_{device}, and s.d. of the truncated normal distribution for ET choice, SD_{choice}) from the model produced for the escape response of *P. major* (i.e., D_{attack}=34.73 mm, U_{pred}=1.54 m s^{-1}, R_{device}=199 mm, SD_{choice}=0.33). Using the model where the predator can adjust the strike path (Appendix 1—figure 1B), we simulate the situation in which the safety zone shape inside the predator's turning

759 radius is similar to the Corcoran's model (Appendix 1—figure 1A) but we included a safety zone
760 opposite to the incoming direction of the predator. We considered D_{attack} as 400 mm, $D_{initial}$ as 130
761 mm, the minimum turning radius of the predator R_{turn} as 12 mm, and the reaction distance of the
762 predator D_{react} as 70 mm. We used the same values of the *P. major* model for R_{device} and the other
763 parameters. We then fixed four parameters and varied the fifth parameter (U_{pred}, D_{attack}, $D_{initial}$, R_{turn},
764 SD_{choice}) to examine the effect of each parameter on the ET distribution.
765
766 **Data availability**
767 The datasets (Dataset1–5) of the escape response in *P. major*, used for statistical analysis and figures,
768 and the R code (Source code 1–3) for the mathematical model, statistical analysis, and figures are
769 available in Figshare: https://figshare.com/s/bea4ee4e7f7664ccd80c.
770
771 **Acknowledgements**
772 We sincerely thank Y. Y. Watanabe for his constructive comments on an early version of this paper.
773 We appreciate the valuable comments from A. D. Bolton, C. Rutz, and an anonymous reviewer,
774 which significantly improved the manuscript. We also thank H. Kamihata for providing equipment
775 for rearing *P. major*. This study was funded by Grants-in-Aid for Scientific Research, Japan Society
776 for the Promotion of Science, to Y.K. (17K17949 and 19H04936), Sumitomo Foundation to Y.K.
777 (153128), and the ISM Cooperative Research Program to Y.K. and K.S (2014-ISM.CRP-2006).
778
779 **Competing interests**
780 Authors declare no competing interests.
781
782 ## References
783 1. Bullock TH. Comparative neuroethology of startle, rapid escape, and giant fiber-mediated
784 responses. In: Eaton RC, editor. Neural mechanisms of startle behavior. Boston, MA: Springer; 1984. p.
785 1-13.
786 2. Cooper WE, Blumstein DT. Escaping from predators. Cambridge, UK: Cambridge University
787 Press; 2015. 442 p.
788 3. Meager JJ, Domenici P, Shingles A, Utne-Palm AC. Escape responses in juvenile Atlantic cod
789 *Gadus morhua* L.: the effects of turbidity and predator speed. J Exp Biol. 2006;209(20):4174-84. doi:
790 10.1242/jeb.02489.
791 4. Arnott SA, Neil DM, Ansell AD. Escape trajectories of the brown shrimp *Crangon crangon*, and a

792 theoretical consideration of initial escape angles from predators. J Exp Biol. 1999;202(2):193-209. doi:
793 10.1242/jeb.202.2.193.
794 5. Bateman PW, Fleming PA. Switching to Plan B: Changes in the escape tactics of two grasshopper
795 species (Acrididae: Orthoptera) in response to repeated predatory approaches. Behav Ecol Sociobiol.
796 2014;68(3):457-65. doi: 10.1007/s00265-013-1660-0.
797 6. Hein AM, Gil MA, Twomey CR, Couzin ID, Levin SA. Conserved behavioral circuits govern
798 high-speed decision-making in wild fish shoals. Proc Natl Acad Sci USA. 2018;115(48):12224-8. doi:
799 10.1073/pnas.1809140115.
800 7. Broom M, Ruxton GD. You can run - or you can hide: Optimal strategies for cryptic prey against
801 pursuit predators. Behav Ecol. 2005;16(3):534-40. doi: 10.1093/beheco/ari024.
802 8. Cooper WE, Pérez-Mellado V, Baird T, Baird TA, Caldwell JP, Vitt LJ. Effects of risk, cost, and
803 their interaction on optimal escape by nonrefuging Bonaire whiptail lizards, *Cnemidophorus murinus*.
804 Behav Ecol. 2003;14(2):288-93. doi: 10.1093/beheco/14.2.288.
805 9. Walker JA, Ghalambor CK, Griset OL, McKenney D, Reznick DN. Do faster starts increase the
806 probability of evading predators? Funct Ecol. 2005;19(5):808-15. doi: 10.1111/j.1365-2435.2005.01033.x.
807 10. Shifferman E, Eilam D. Movement and direction of movement of a simulated prey affect the
808 success rate in barn owl *Tyto alba* attack. J Avian Biol. 2004;35(2):111-6. doi:
809 10.1111/j.0908-8857.2004.03257.x.
810 11. Camhi JM, Tom W, Volman S. The escape behavior of the cockroach *Periplaneta americana*- II.
811 Detection of natural predators by air displacement. J Comp Physiol A Sens Neural Behav Physiol.
812 1978;128(3):203-12. doi: 10.1007/bf00656853.
813 12. Kimura H, Kawabata Y. Effect of initial body orientation on escape probability of prey fish
814 escaping from predators. Biol Open. 2018;7(7):bio023812. doi: 10.1242/bio.023812.
815 13. Dangles O, Ory N, Steinmann T, Christides JP, Casas J. Spider's attack versus cricket's escape:
816 velocity modes determine success. Anim Behav. 2006;72(3):603-10. doi: 10.1016/j.anbehav.2005.11.018.
817 14. Weihs D, Webb PW. Optimal avoidance and evasion tactics in predator-prey interactions. J Theor
818 Biol. 1984;106(2):189-206. doi: 10.1016/0022-5193(84)90019-5.
819 15. Domenici P. The visually mediated escape response in fish: predicting prey responsiveness and
820 the locomotor behaviour of predators and prey. Mar Freshwat Behav Physiol. 2002;35(1-2):87-110. doi:
821 10.1080/10236240290025635.
822 16. Jensen G. Behavioral Stochasticity. Encyclopedia of Animal Cognition and Behavior. Cham:
823 Springer; 2018. p. 1-5.
824 17. Domenici P, Blagburn JM, Bacon JP. Animal escapology I: Theoretical issues and emerging
825 trends in escape trajectories. J Exp Biol. 2011;214(15):2463-73. doi: 10.1242/jeb.029652.
826 18. Soto A, Stewart WJ, McHenry MJ. When optimal strategy matters to prey fish. Integr Comp Biol.
827 2015;55(1):110-20. doi: 10.1093/icb/icv027.
828 19. Humphries DA, Driver PM. Protean defence by prey animals. Oecologia. 1970;5(4):285-302. doi:
829 10.1007/bf00815496.

20. Jones KA, Jackson AL, Ruxton GD. Prey jitters; protean behaviour in grouped prey. Behav Ecol. 2011;22(4):831-6. doi: 10.1093/beheco/arr062.
21. Richardson G, Dickinson P, Burman OHP, Pike TW. Unpredictable movement as an anti-predator strategy. Proc R Soc Lond B. 2018;285(1885). doi: 10.1098/rspb.2018.1112.
22. Moore TY, Cooper KL, Biewener AA, Vasudevan R. Unpredictability of escape trajectory explains predator evasion ability and microhabitat preference of desert rodents. Nature Communications. 2017;8(1). doi: 10.1038/s41467-017-00373-2.
23. Howland HC. Optimal strategies for predator avoidance: The relative importance of speed and manoeuvrability. J Theor Biol. 1974;47(2):333-50. doi: 10.1016/0022-5193(74)90202-1.
24. Corcoran AJ, Conner WE. How moths escape bats: predicting outcomes of predator-prey interactions. J Exp Biol. 2016;219:2704-15. doi: 10.1242/jeb.137638.
25. Martin BT, Gil MA, Fahimipour AK, Hein AM. Informational constraints on predator–prey interactions. Oikos. 2022;2022(10):e08143. doi: 10.1111/oik.08143.
26. Domenici P, Blagburn JM, Bacon JP. Animal escapology II: Escape trajectory case studies. J Exp Biol. 2011;214(15):2474-94. doi: 10.1242/jeb.053801.
27. Cooper WE. Risk factors and escape strategy in the grasshopper *Dissosteira carolina*. Behaviour. 2006;143(10):1201-18. doi: 10.1163/156853906778691595.
28. Domenici P, Blake RW. Escape trajectories in angelfish (*Pterophyllum eimekei*). J Exp Biol. 1993;177:253-72. doi: 10.1242/jeb.177.1.253.
29. Domenici P, Booth D, Blagburn JM, Bacon JP. Cockroaches keep predators guessing by using preferred escape trajectories. Curr Biol. 2008;18(22):1792-6. doi: 10.1016/j.cub.2008.09.062.
30. Reed DD, Kaplan BA. The matching law: A tutorial for practitioners. Behav Anal Pract. 2011;4(2):15-24. doi: 10.1007/BF03391780.
31. Poling A, Edwards TL, Weeden M, Foster TM. The matching law. Psycol Rec. 2011;61(2):313-22. doi: 10.1007/BF03395762.
32. McDowell JJ. On the theoretical and empirical status of the matching law and matching theory. Psychol Bull. 2013;139(5):1000-28. doi: 10.1037/a0029924.
33. Houston AI, Trimmer PC, McNamara JM. Matching behaviours and rewards. Trends Cogn Sci. 2021;25(5):403-15. doi: 10.1016/j.tics.2021.01.011.
34. Fawcett TW, Hamblin S, Giraldeau LA. Exposing the behavioral gambit: the evolution of learning and decision rules. Behav Ecol. 2012;24(1):2-11. doi: 10.1093/beheco/ars085.
35. Webb PW, Skadsen JM. Strike tactics of *Esox*. Can J Zool. 1980;58(8):1462-9. doi: 10.1139/z80-201.
36. Fouts WR, Nelson DR. Prey capture by the pacific angel shark, *Squatina californica*: visually mediated strikes and ambush-site characteristics. Copeia. 1999;1999(2):304-12. doi: 10.2307/1447476.
37. Anderson CW. The modulation of feeding behavior in response to prey type in the frog *Rana pipiens*. J Exp Biol. 1993;179(1):1-12. doi: 10.1242/jeb.179.1.1.
38. Paglianti A, Domenici P. The effect of size on the timing of visually mediated escape behaviour in

868 staghorn sculpin *Leptocottus armatus*. J Fish Biol. 2006;68:1177-91. doi:
869 10.1111/j.1095-8649.2006.00991.x.
870 39. Fabian ST, Sumner ME, Wardill TJ, Rossoni S, Gonzalez-Bellido PT. Interception by two
871 predatory fly species is explained by a proportional navigation feedback controller. J R Soc Lond Interface.
872 2018;15(147). doi: 10.1098/rsif.2018.0466.
873 40. Domenici P, Blake RW. The kinematics and performance of the escape response in the angelfish
874 (*Pterophyllum eimekei*). J Exp Biol. 1991;156:187-205. doi: 10.1242/jeb.156.1.187.
875 41. Danos N, Lauder GV. Challenging zebrafish escape responses by increasing water viscosity. J
876 Exp Biol. 2012;215(11):1854-62. doi: 10.1242/jeb.068957.
877 42. Fleuren M, van Leeuwen JL, Quicazan-Rubio EM, Pieters RPM, Pollux BJA, Voesenek CJ.
878 Three-dimensional analysis of the fast-start escape response of the least killifish, *Heterandria formosa*. J
879 Exp Biol. 2018;221(7). doi: 10.1242/jeb.168609.
880 43. Ellerby DJ, Altringham JD. Spatial variation in fast muscle function of the rainbow trout
881 *Oncorhynchus mykiss* during fast-starts and sprinting. J Exp Biol. 2001;204(13):2239-50. doi:
882 10.1242/jeb.204.13.2239.
883 44. Domenici P, Blake RW. The kinematics and performance of fish fast-start swimming. J Exp Biol.
884 1997;200(8):1165-78. doi: 10.1242/jeb.200.8.1165.
885 45. Weihs D. The mechanism of rapid starting of slender fish. Biorheology. 1973;10(3):343-50. doi:
886 10.3233/bir-1973-10308.
887 46. Domenici P, Booth D, Blagburn JM, Bacon JP. Escaping away from and towards a threat: The
888 cockroach's strategy for staying alive. Communicative and Integrative Biology. 2009;2(6):497-500. doi:
889 10.4161/cib.2.6.9408.
890 47. Nair A, Changsing K, Stewart WJ, McHenry MJ. Fish prey change strategy with the direction of
891 a threat. Proc R Soc Lond B. 2017;284(1857). doi: 10.1098/rspb.2017.0393.
892 48. Kanou M, Ohshima M, Inoue J. The air-puff evoked escape behavior of the cricket *Gryllus*
893 *bimaculatus* and its compensational recovery after cercal ablations. Zool Sci. 1999;16(1):71-9. doi:
894 10.2108/zsj.16.71.
895 49. Fuiman LA. Development of predator evasion in Atlantic herring, *Clupea harengus* L. Anim
896 Behav. 1993;45(6):1101-16. doi: 10.1006/anbe.1993.1135.
897 50. Martín J, López P. The escape response of juvenile *Psammodromus algirus* lizards. J Comp
898 Psychol. 1996;110(2):187-92. doi: 10.1037/0735-7036.110.2.187.
899 51. Bulbert MW, Page RA, Bernal XE. Danger comes from all fronts: Predator-dependent escape
900 tactics of túngara frogs. PLoS ONE. 2015;10(4):e0120546. doi: 10.1371/journal.pone.0120546.
901 52. Domenici P, Batty RS. Escape behaviour of solitary herring (*Clupea harengus*) and comparisons
902 with schooling individuals. Mar Biol. 1997;128(1):29-38. doi: 10.1007/s002270050065.
903 53. Szopa-Comley AW, Ioannou CC. Responsive robotic prey reveal how predators adapt to
904 predictability in escape tactics. Proc Natl Acad Sci U S A. 2022;119(23):e2117858119. doi:
905 10.1073/pnas.2117858119.

906 54. Eaton RC, Lee RKK, Foreman MB. The Mauthner cell and other identified neurons of the
907 brainstem escape network of fish. Prog Neurobiol. 2001;63(4):467-85. doi: 10.1016/s0301-0082(00)00047-2.
908 55. Yono O, Shimozawa T. Synchronous firing by specific pairs of cercal giant interneurons in
909 crickets encodes wind direction. Biosystems. 2008;93(3):218-25. doi: 10.1016/j.biosystems.2008.04.014.
910 56. Card GM. Escape behaviors in insects. Curr Opin Neurobiol. 2012;22(2):180-6. doi:
911 10.1016/j.conb.2011.12.009.
912 57. Levi R, Camhi JM. Population vector coding by the giant interneurons of the cockroach. J
913 Neurosci. 2000;20(10):3822-9. doi: 10.1523/JNEUROSCI.20-10-03822.2000.
914 58. Stewart WJ, Nair A, Jiang H, McHenry MJ. Prey fish escape by sensing the bow wave of a
915 predator. J Exp Biol. 2014;217(24):4328-36. doi: 10.1242/jeb.111773.
916 59. Bhattacharyya K, McLean DL, MacIver MA. Visual threat assessment and reticulospinal
917 encoding of calibrated responses in larval zebrafish. Curr Biol. 2017;27(18):2751-62 e6. doi:
918 10.1016/j.cub.2017.08.012.
919 60. Akanyeti O, Putney J, Yanagitsuru YR, Lauder GV, Stewart WJ, Liao JC. Accelerating fishes
920 increase propulsive efficiency by modulating vortex ring geometry. Proc Natl Acad Sci USA.
921 2017;114(52):13828-33. doi: 10.1073/pnas.1705968115.
922 61. Webster MM, Rutz C. How STRANGE are your study animals? Nature. 2020;582:337-40. doi:
923 10.1038/d41586-020-01751-5.
924 62. Moore TY, Biewener AA. Outrun or outmaneuver: predator–prey interactions as a model system
925 for integrating biomechanical studies in a broader ecological and evolutionary context. Integr Comp Biol.
926 2015;55(6):1188-97. doi: 10.1093/icb/icv074.
927 63. Rand DM, Lauder GV. Prey capture in the chain pickerel, *Esox niger*: correlations between
928 feeding and locomotor behavior. Can J Zool. 1981;59(6):1072-8. doi: 10.1139/z81-149.
929 64. Stewart WJ, Cardenas GS, McHenry MJ. Zebrafish larvae evade predators by sensing water flow.
930 J Exp Biol. 2013;216(3):388-98. doi: 10.1242/jeb.072751.
931 65. Batschelet E. Circular statistics in biology. New York: Academic Press; 1981. 371 p.
932 66. Law CSW, Sadovy de Mitcheson Y. Reproductive biology of black seabream *Acanthopagrus*
933 *schlegelii*, threadfin porgy *Evynnis cardinalis* and red pargo *Pagrus major* in the northern South China
934 Sea with consideration of fishery status and management needs. J Fish Biol. 2017;91(1):101-25. doi:
935 10.1111/jfb.13331.
936 67. Miyajima-Taga Y, Masuda R, Kurihara A, Yamashita Y, Takeuchi T. Feeding moon jellyfish
937 improves the tilting behavior of hatchery-reared red sea bream juveniles. Nippon Suisan Gakkaishi (in
938 Japanese with English abstract). 2014;80(6):934-45. doi: 10.2331/suisan.80.934.
939 68. Kudoh T, Sawa K, Yamaoka K. Settlement of wild juvenile red sea bream (*Pagrus major*) around
940 two types of artificial habitat. Nippon Suisan Gakkaishi (in Japanese with English abstract). 2002. doi:
941 10.2331/suisan.68.874.
942 69. Zuur A, Ieno EN, Walker N, Saveliev AA, Smith GM. Mixed effects models and extensions in
943 ecology with R. New York: Springer; 2009. 574 p.

70. Brilleman SL, Howe LD, Wolfe R, Tilling K. Bayesian piecewise linear mixed models with a random change point: an application to BMI rebound in childhood. Epidemiology. 2017;28(6):827-33. doi: 10.1097/EDE.0000000000000723.

71. Kéry M, Schaub M. Bayesian population analysis using winbugs – a hierarchical perspective. Burlington: Academic Press; 2011. 535 p.

72. Zar JH. Biostatistical analysis: fifth edition. New Jersey: Pearson Education; 2010. 944 p.

Figure supplements

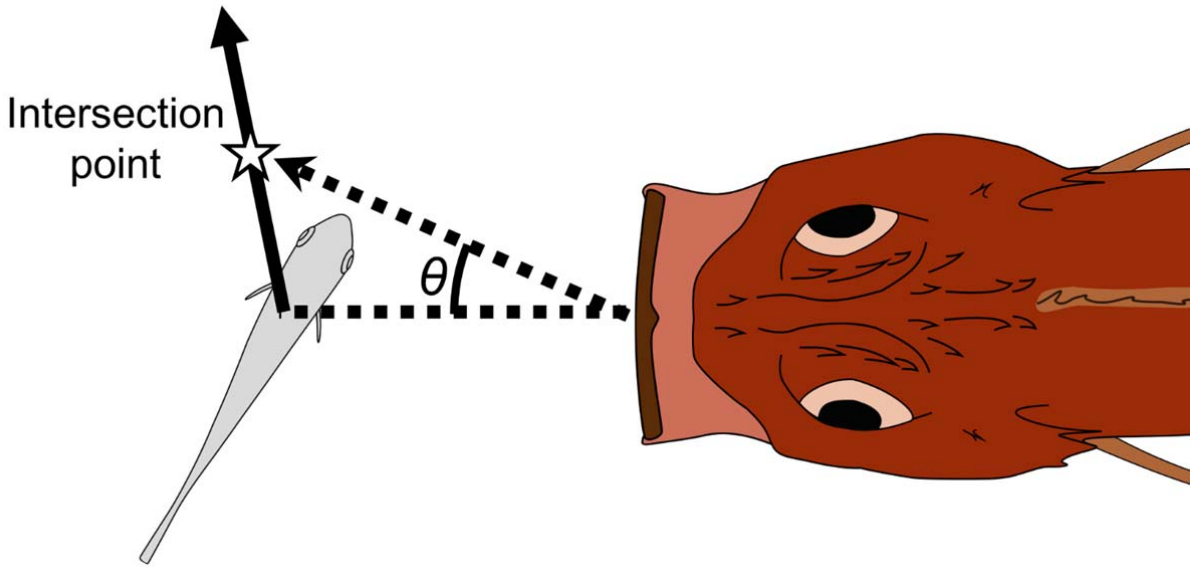

Figure 2—figure supplement 1. Schematic drawing of how the adjusted angle of the predator (θ) was measured. The intersection point is the crossing point between the trajectory of the prey's center of mass (CoM) and the trajectory of the predator's tip of the mouth. The adjusted angle is defined as the angle between the line passing through the predator's tip of the mouth and the prey's CoM at the onset of the prey's escape response, and the line passing through the predator's tip of the mouth at the onset of the escape response and the intersection point.

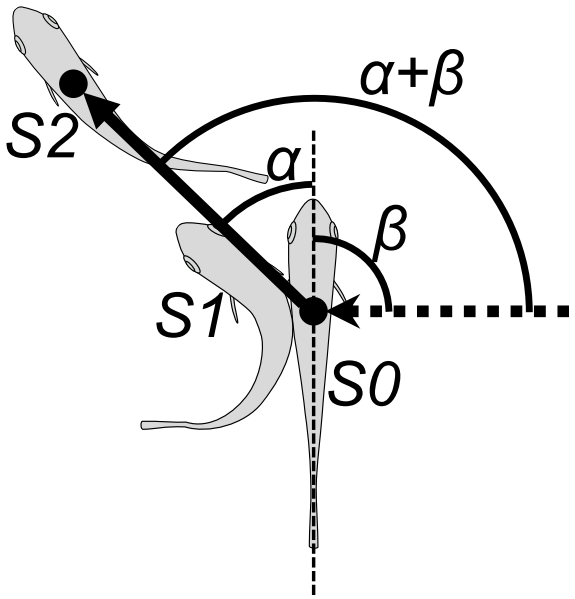

Figure 2—figure supplement 2. Schematic drawing of angular variables. *Filled circle* position of the center of mass; *Dotted arrow* approach direction of the dummy predator; *S0* position of the fish at the onset of stage 1, *S1* position at the end of stage 1, *S2* position at the end of stage 2, α turn angle, β initial orientation, $\alpha+\beta$ escape trajectory (ET).

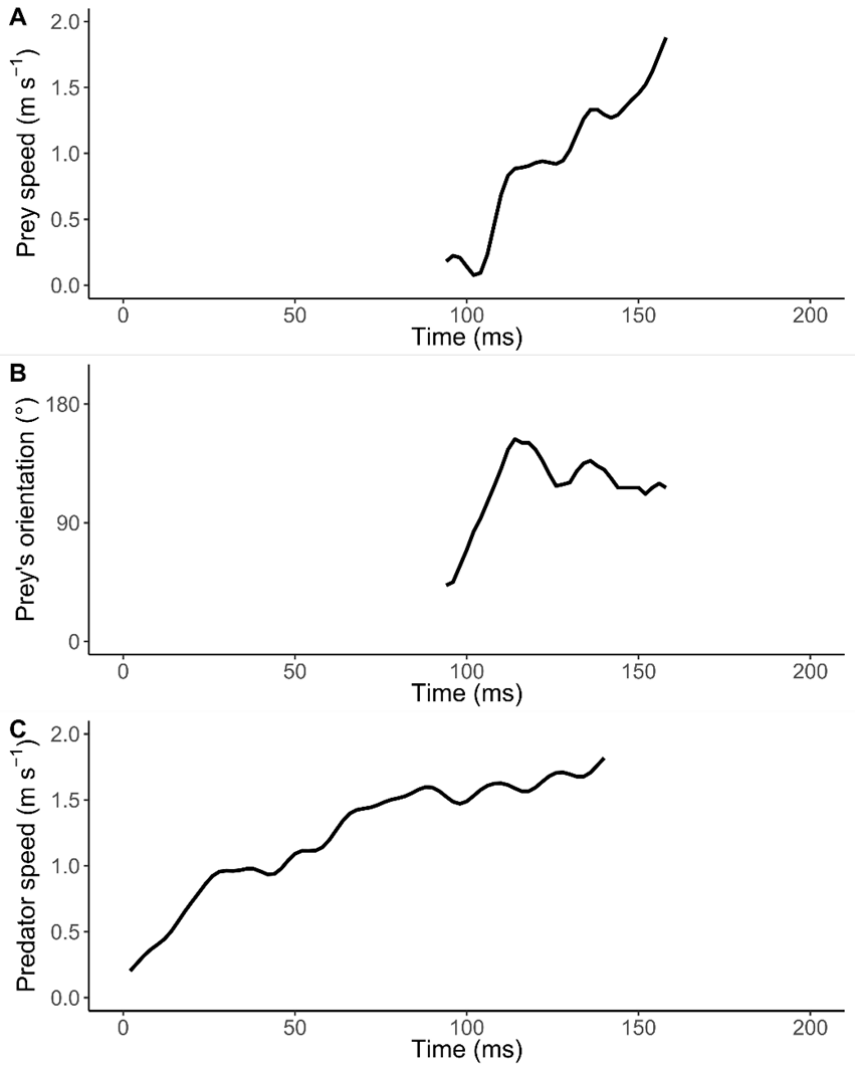

Figure 3—figure supplement 1. Representatives of kinematic variables of the prey *Pagrus major* and the predator over time. (A) Prey speed after the onset of escape response. (B) Prey's body orientation relative to the predator's approach path after the onset of escape response. (C) Speed of the approaching dummy predator. The speeds of the prey and the predator were calculated by first-order differentiation of the cumulative distance for the time series using a Lanczos five-point quadratic moving regression method.

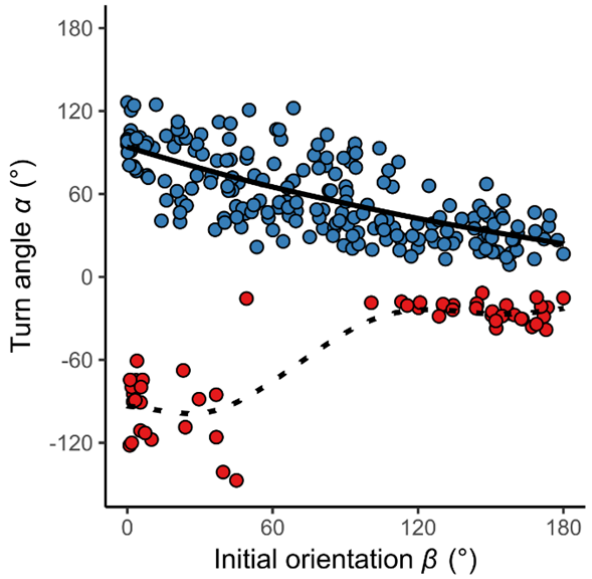

Figure 3—figure supplement 2. Relationship between initial orientation β and turn angle α in the experiment. Different colors represent the away (blue) and toward (red) responses. Solid and dotted lines are estimated by the generalized additive mixed model (GAMM). The dataset and R code are available at Figshare ("Dataset1.csv" and "Source code 1.R") [n=264 (208 away and 56 toward responses) from 23 individuals].

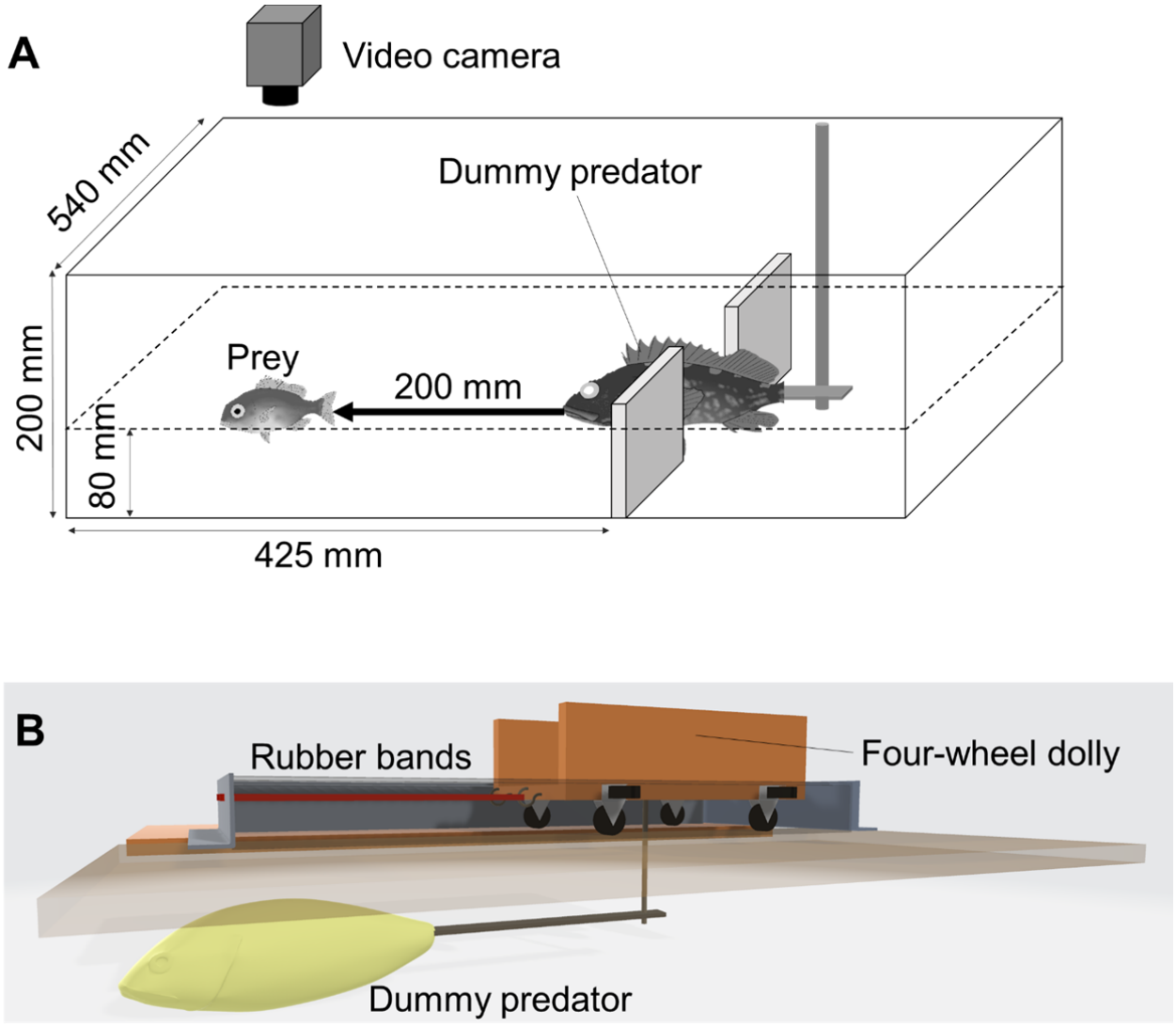

979

980 **Figure 3—figure supplement 3.** Experimental apparatus. (A) Sketch of the experimental tank for
981 measuring the escape response of prey fish *Pagrus major*. (B) Sketch (3D model) of the actuation system of
982 the dummy predator.

983

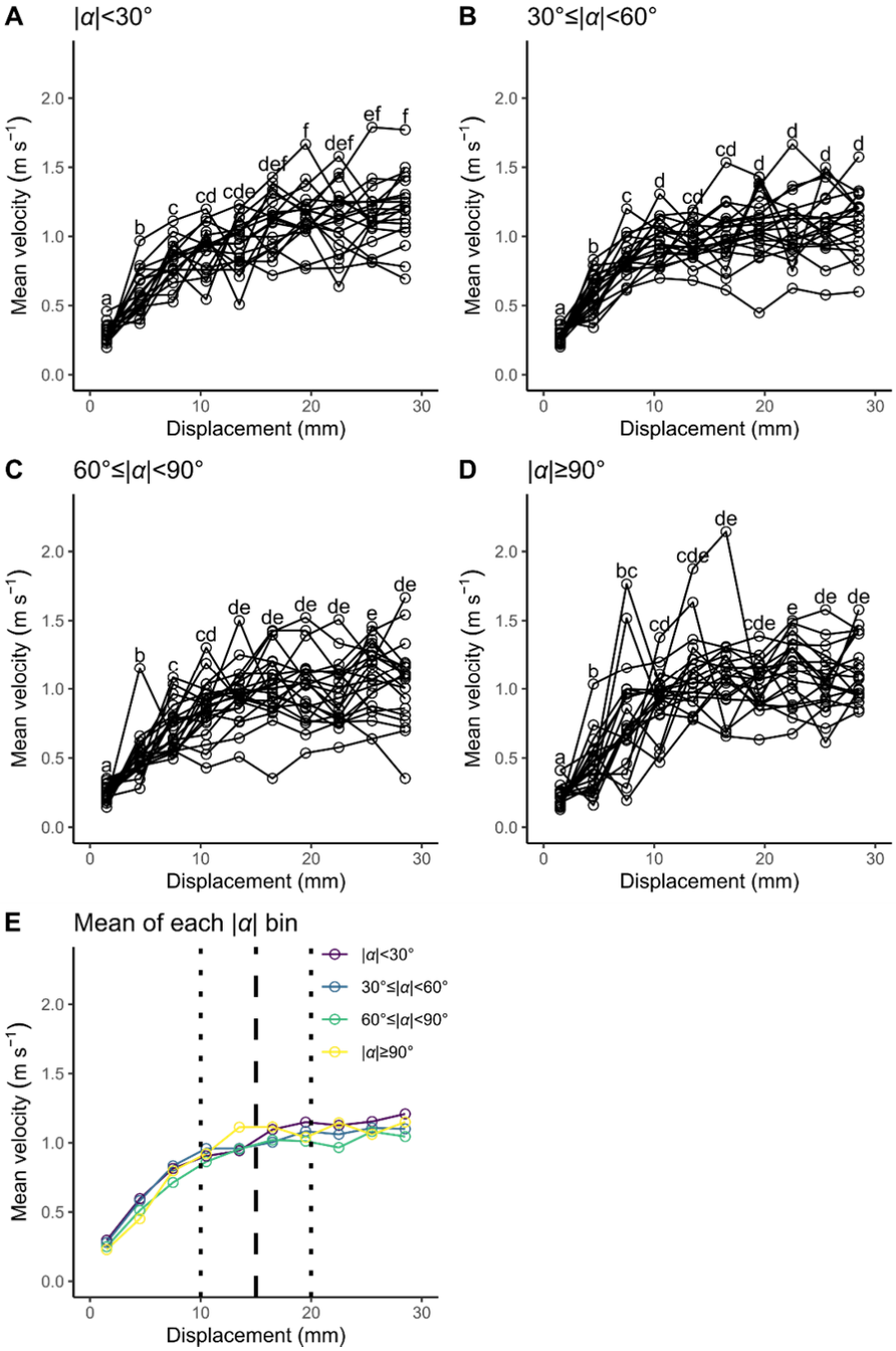

Figure 4—figure supplement 1. Relationship between displacement from the initial position (3-mm intervals: 0–3, 3–6, ..., and 27–30 mm) and mean velocity during the displacement for each turn angle (|α|) bin. Unfilled circles denote the mean value for each individual. Different lowercase letters represent significant differences according to the paired *t*-test with Bonferroni's correction (P<0.05). (A) |α|<30°. (B) 30°≤|α|<60°. (C) 60°≤|α|<90°. (D) |α|≥90°. (E) Mean of the individual mean value for each |α| bin. Vertical dashed line represents the cut-off distance of 15 mm used in this study, and vertical dotted lines represent the other cut-off distances tested in this study (Table 2—source data 1 and Table 3—source data 2). The datasets and R code are available at Figshare ("Dataset1.csv", "Dataset2.csv", "Dataset3.csv", and "Source code 1.R") (n=23 individuals).

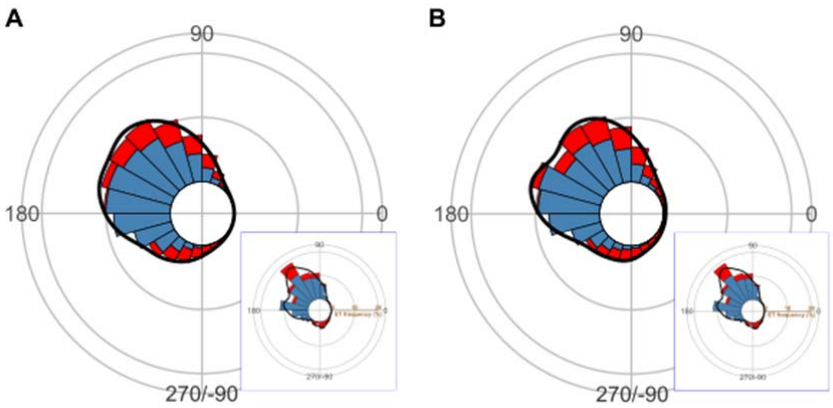

Figure 5—figure supplement 1. Circular histogram of the theoretical escape trajectories (ETs), estimated by a Monte Carlo simulation of the model that uses the dummy predator speed per trial [(A) the predator speed at the onset of escape response of prey; (B) the mean predator speed to cover 75% of the flight initiation distance of prey]. The probability of selection of an ET was determined by the truncated normal distribution of the optimal ranking index. This process was repeated 1000 times to estimate the frequency distribution of the theoretical ETs. Colors in the bars represent the away (blue) or toward (red) responses. Black lines represent the kernel probability density function. Concentric circles represent 10 % of the total sample sizes, the bin intervals are 15°, and the bandwidths of the kernel are 50. The predator's approach direction is represented by 0°. The resulting ETs (A and B) are statistically different from the observed ETs (lower right panel of each figure), which show clear multiple peaks. This demonstrates that the prey fish do not choose ETs based on the predator speed. The dataset and R code are available at Figshare ("Dataset1.csv" and "Source code 1.R") [(A) n=264 per simulation ×1000 times; (B) n=257 per simulation ×1000 times; note that the sample size is smaller than the total number of observations, 264, because the dummy predator did not move over 75 % of the flight initiation distance of prey in seven cases).

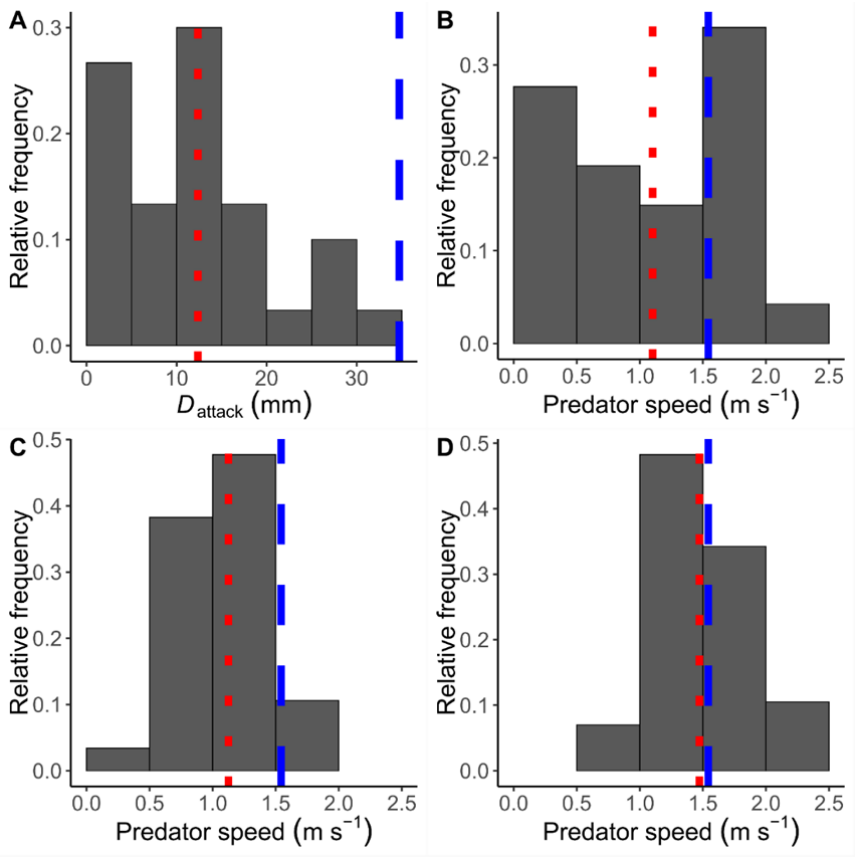

Figure 5—figure supplement 2. Predator *Sebastiscus marmoratus* attack parameters. (A) Histogram of the distance between the prey's initial position and the predator's mouth position at the onset of the mouth closing (D_{attack}) (n=30 from 7 individuals). (B) Histogram of the speed of the real predator (n=47 from 7 individuals). (C) Histogram of the dummy predator speed at the onset of escape response of prey (n=264 from 23 individuals). (D) Histogram of the dummy predator speed to cover 75 % of the prey's flight initiation distance (n=257 from 23 individuals; Note that the sample size is smaller than the total number of observations, 264, because the dummy predator did not move over 75 % of the prey's flight initiation distance in seven cases). Figures A and B are based on reanalysis of data from Kimura and Kawabata [12]. Figures C and D are based on the experiment in this study. Vertical dashed blue lines represent the optimal values independently estimated in this study, and vertical dotted red lines represent the mean values of the real or dummy predator. The datasets and R code are available at Figshare ("Dataset1.csv", "Dataset4.csv", "Dataset5.csv", and "Source code 1.R").

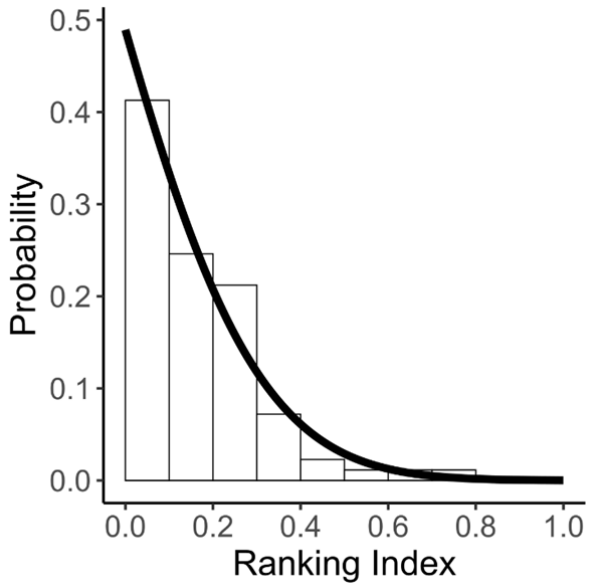

Figure 5—figure supplement 3. Histogram of the ranking index, where 0 indicates that the real fish chose the theoretically optimal escape trajectory (ET) and 1 indicates that the real fish chose the theoretically worst ET. The solid line is the density probability function of the truncated normal distribution. The dataset and R code are available at Figshare ("Dataset1.csv" and "Source code 1.R") (n=264 from 23 individuals).

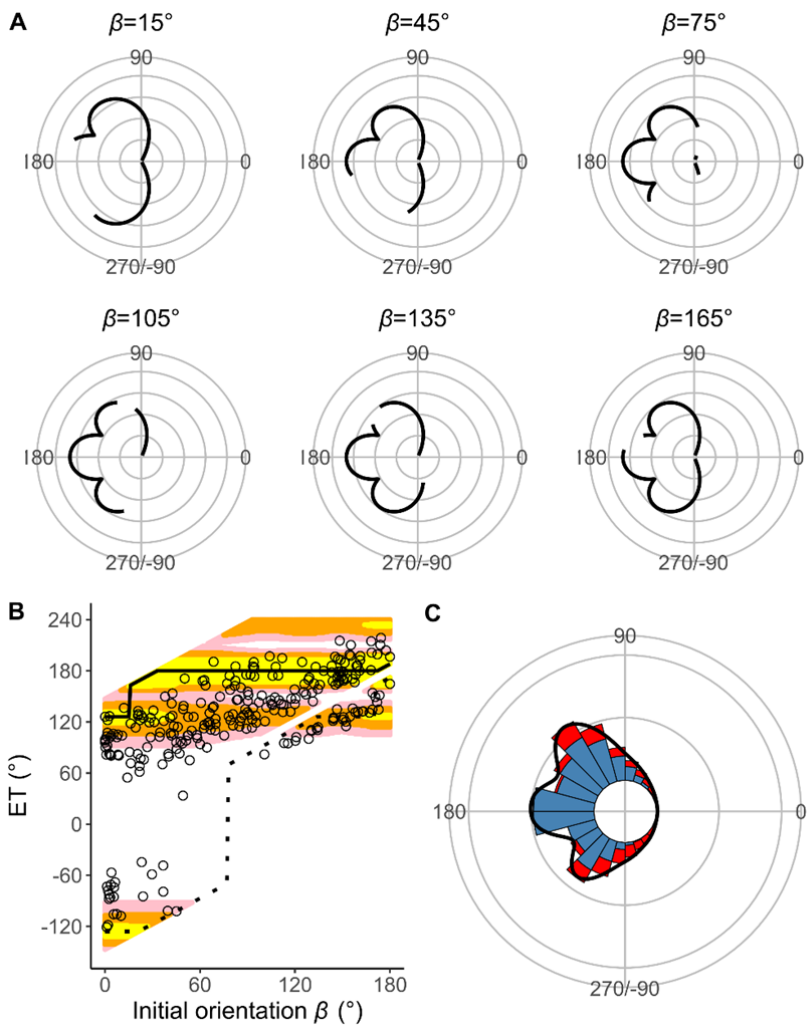

Figure 5—figure supplement 4. Estimates of the model with D_{attack} (the distance between the prey's initial position and the endpoint of the predator attack) and without $T_1(|\alpha|)$ (the relationship between the absolute value of the turn angle $|\alpha|$ and the time required for a 15-mm displacement from the initial position, or the time required for prey to turn). (A) Circular plots of the time difference between the prey and predator T_{diff} in different initial orientations β. The time difference of the best escape trajectory (ET) was regarded as 10 ms, and the relative time differences between 0 and 10 ms are shown by solid lines. Areas without solid lines indicate that either the time difference is below 0 or the fish cannot go to that ET because of the constraint on the possible range of $|\alpha|$. Concentric circles represent 3 ms. (B) Relationship between the initial orientation β and ET. Solid and dotted lines represent the best-estimated away and toward responses, respectively. Different colors represent the top 10%, 25%, and 40% quantiles of the time difference between the prey and predator within all possible ETs. (C) Circular histogram of the theoretical ETs, estimated by a Monte Carlo simulation. The probability of selection of an ET was determined by the truncated normal distribution of the optimal ranking index. This process was repeated 1000 times to estimate the frequency distribution of the theoretical ETs. Colors in the bars represent the away (blue) or toward (red) responses. Black lines represent the kernel probability density function. Concentric circles represent 10 % of the total sample sizes, the bin intervals are 15°, and the bandwidths of the kernel are 50. The predator's approach direction is represented by 0°. The dataset and R code are available at Figshare ("Dataset1.csv" and "Source code 1.R") (n=264 from 23 individuals for experimental data, and n=264000 for Monte Carlo simulation).

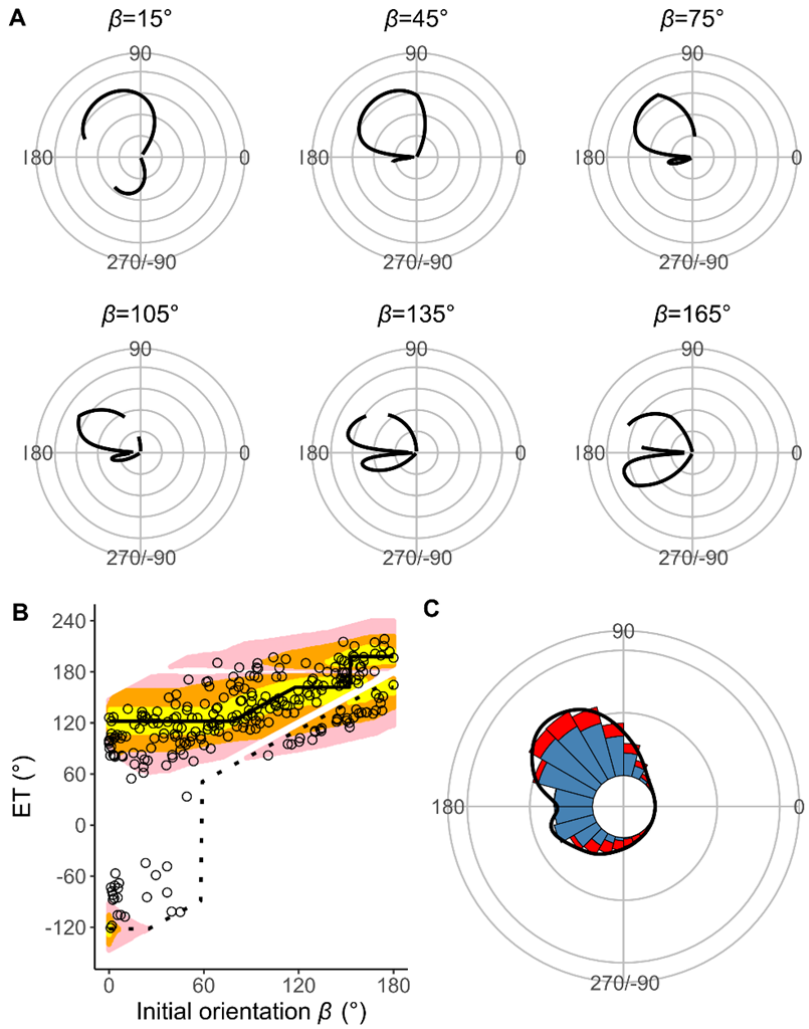

Figure 5—figure supplement 5. Estimates of the model with $T_1(|\alpha|)$ (the relationship between the absolute value of the turn angle $|\alpha|$ and the time required for a 15-mm displacement from the initial position, or the time required for the prey to turn) and without D_{attack} (the distance between the prey's initial position and the endpoint of the predator attack). (A) Circular plots of the time difference between the prey and predator T_{diff} in different initial orientations β. The time difference of the best escape trajectory (ET) was regarded as 10 ms, and the relative time differences between 0 and 10 ms are shown by solid lines. Areas without solid lines indicate that either the time difference is below 0 or the fish cannot go to that ET because of the constraint on the possible range of $|\alpha|$. Concentric circles represent 3 ms. (B) Relationship between the initial orientation β and ET. Solid and dotted lines represent the best-estimated away and toward responses, respectively. Different colors represent the top 10%, 25%, and 40% quantiles of the time difference between the prey and predator within all possible ETs. (C) Circular histogram of the theoretical ETs, estimated by a Monte Carlo simulation. The probability of selection of an ET was determined by the truncated normal distribution of the optimal ranking index. This process was repeated 1000 times to estimate the frequency distribution of the theoretical ETs. Colors in the bars represent the away (blue) or toward (red) responses. Black lines represent the kernel probability density function. Concentric circles represent 10 % of the total sample sizes, the bin intervals are 15°, and the bandwidths of the kernel are 50. The predator's approach direction is represented by 0°. The dataset and R code are available at Figshare ("Dataset1.csv" and "Source code 1.R") (n=264 from 23 individuals for experimental data, and n=264000 for Monte Carlo simulation).

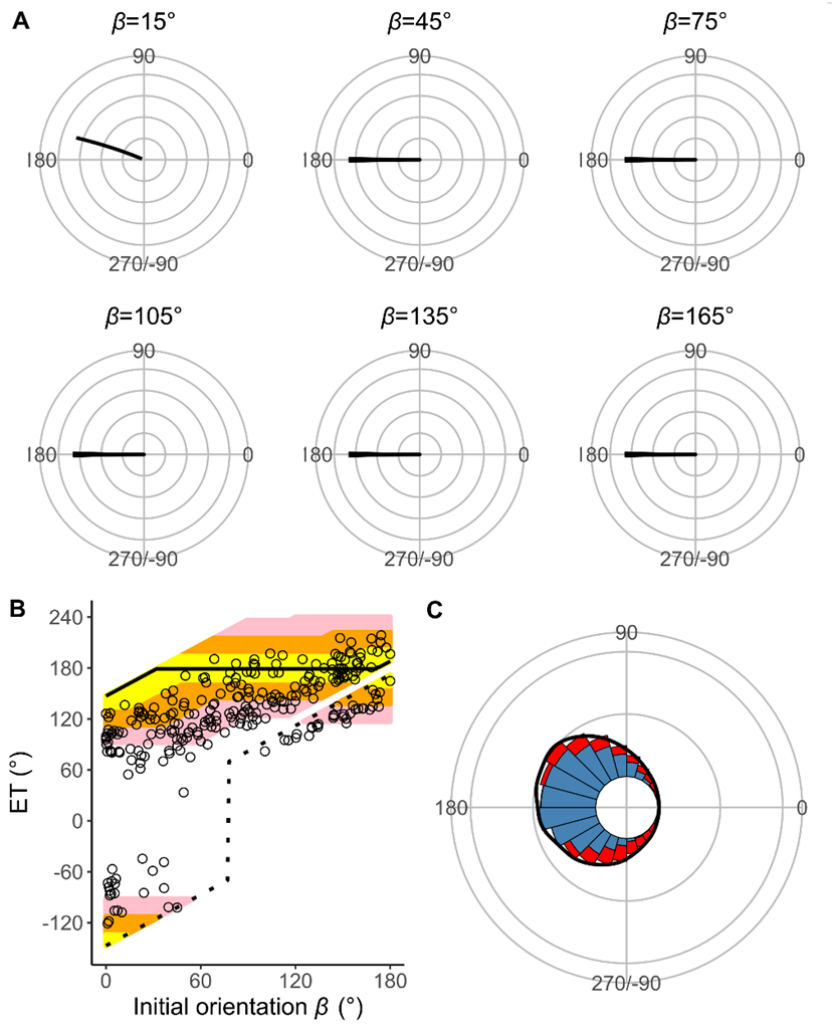

Figure 5—figure supplement 6. Estimates of the model that includes neither D_{attack} (the distance between the prey's initial position and the endpoint of the predator attack) nor $T_1(|\alpha|)$ (the relationship between the absolute value of the turn angle $|\alpha|$ and the time required for a 15-mm displacement from the initial position, or the time required for the prey to turn). (A) Circular plots of the time difference between the prey and predator T_{diff} in different initial orientations β. The time difference of the best escape trajectory (ET) was regarded as 10 ms, and the relative time differences between 0 and 10 ms are shown by solid lines. Areas without solid lines indicate that either the time difference is below 0 or the fish cannot go to that ET because of the constraint on the possible range of $|\alpha|$. Concentric circles represent 3 ms. (B) Relationship between the initial orientation β and ET. Solid and dotted lines represent the best-estimated away and toward responses, respectively. Different colors represent the top 10%, 25%, and 40% quantiles of the time difference between the prey and predator within all possible ETs. (C) Circular histogram of the theoretical ETs, estimated by a Monte Carlo simulation. The probability of selection of an ET was determined by the truncated normal distribution of the optimal ranking index. This process was repeated 1000 times to estimate the frequency distribution of the theoretical ETs. Colors in the bars represent the away (blue) or toward (red) responses. Black lines represent the kernel probability density function. Concentric circles represent 10 % of the total sample sizes, the bin intervals are 15°, and the bandwidths of the kernel are 50. The predator's approach direction is represented by 0°. The dataset and R code are available at Figshare ("Dataset1.csv" and "Source code 1.R") (n=264 from 23 individuals for experimental data, and n=264000 for Monte Carlo simulation).

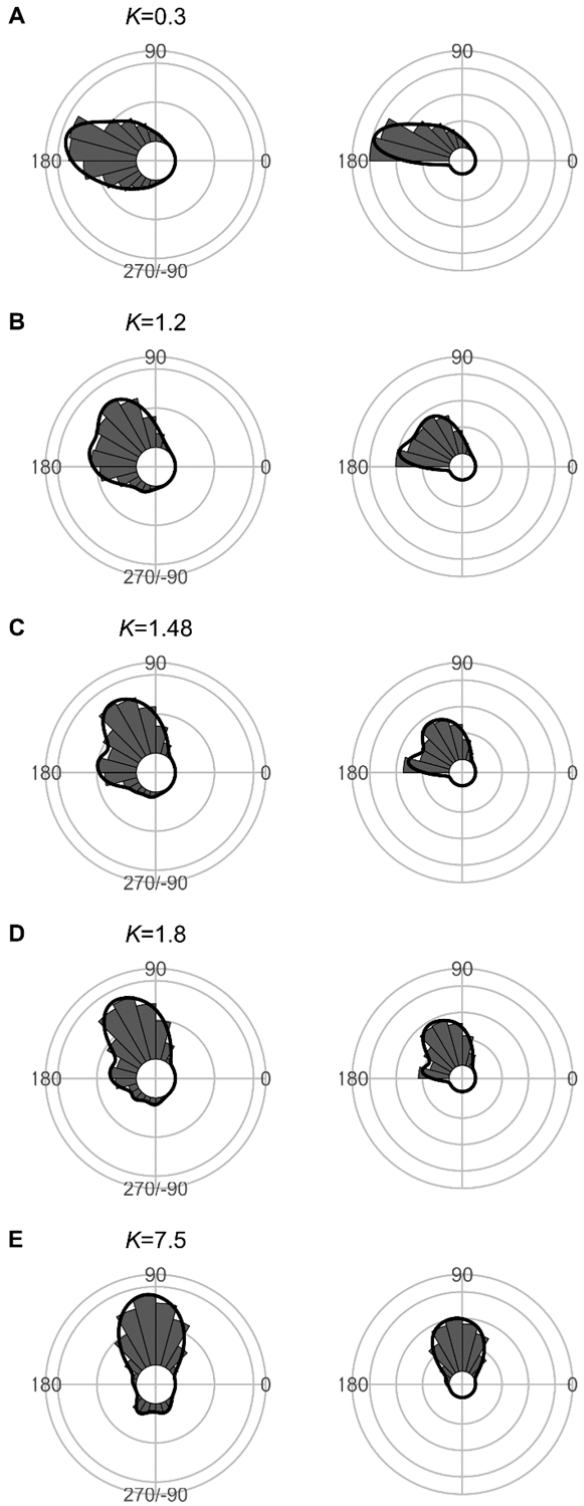

Figure 7—figure supplement 1. Effect of predator speed U_{pred} (K=U_{pred}/U_{prey}) on the theoretical distribution of escape trajectories (ET, left panel; ET_{semi}, right panel). Circular histograms of the theoretical escape trajectories were estimated by a Monte Carlo simulation of the geometric model. ET_{semi} denotes the angle for escape trajectory ranging from 0° (directly toward the threat) to 180° (opposite to the threat), thereby using only one semicircle. The other parameter values are the same as the values used for explaining the escape response of *Pagrus major*. The R code is available at Figshare ("Source code 1.R").

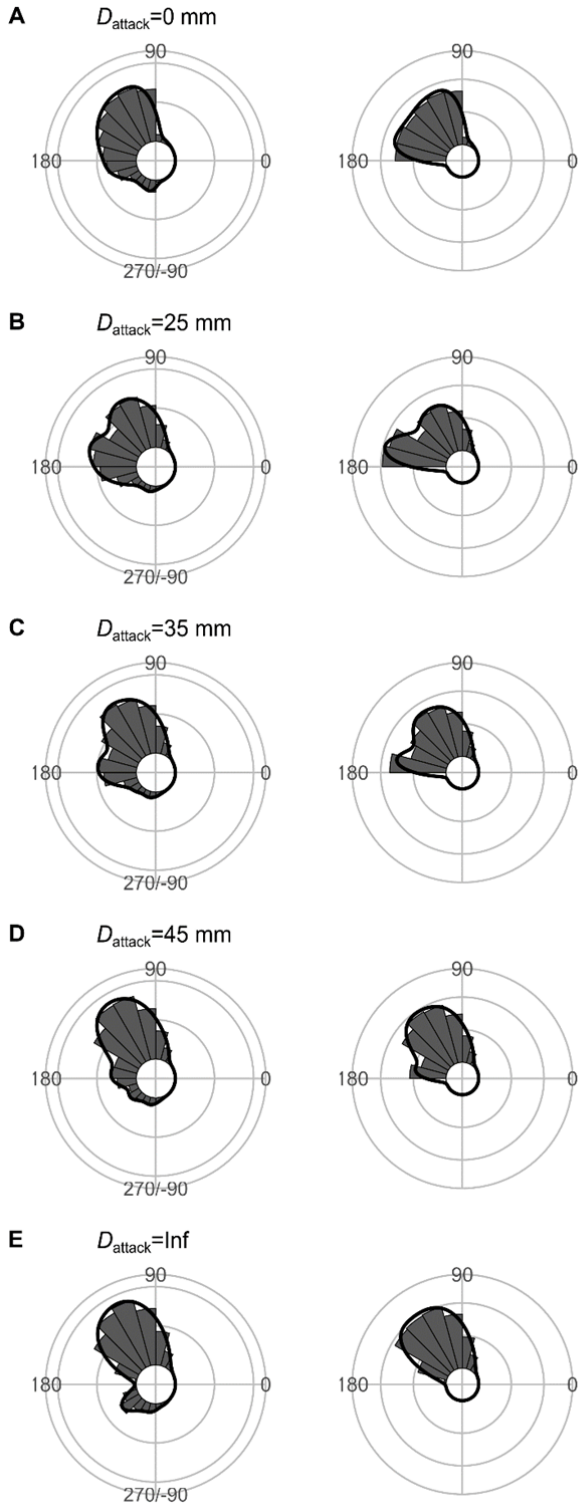

095 **Figure 7—figure supplement 2.** Effect of D_{attack} (the distance between the prey's initial position and the
096 endpoint of the predator attack) on the theoretical distribution of escape trajectories (ET, left panel; ET_{semi},
097 right panel). Circular histograms of the theoretical escape trajectories were estimated by a Monte Carlo
098 simulation of the geometric model. The other parameter values are the same as the values used for
099 explaining the escape response of *Pagrus major*. The R code is available at Figshare ("Source code 1.R").

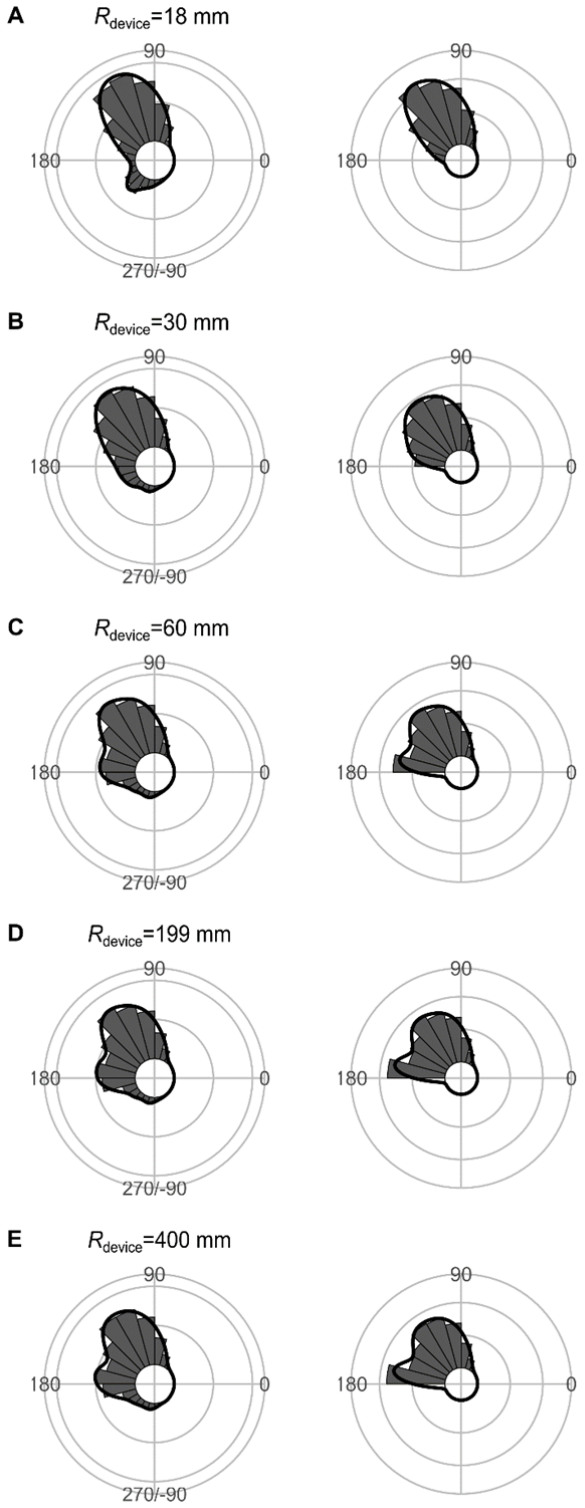

Figure 7—figure supplement 3. Effect of R_{device} (the radius for the shape of the predator's capture device at the moment of attack, which is approximated as an arc) on the theoretical distribution of escape trajectories (ET, left panel; ET_{semi}, right panel). Circular histograms of the theoretical escape trajectories were estimated by a Monte Carlo simulation of the geometric model. The other parameter values are the same as the values used for explaining the escape response of *Pagrus major*. The R code is available at Figshare ("Source code 1.R").

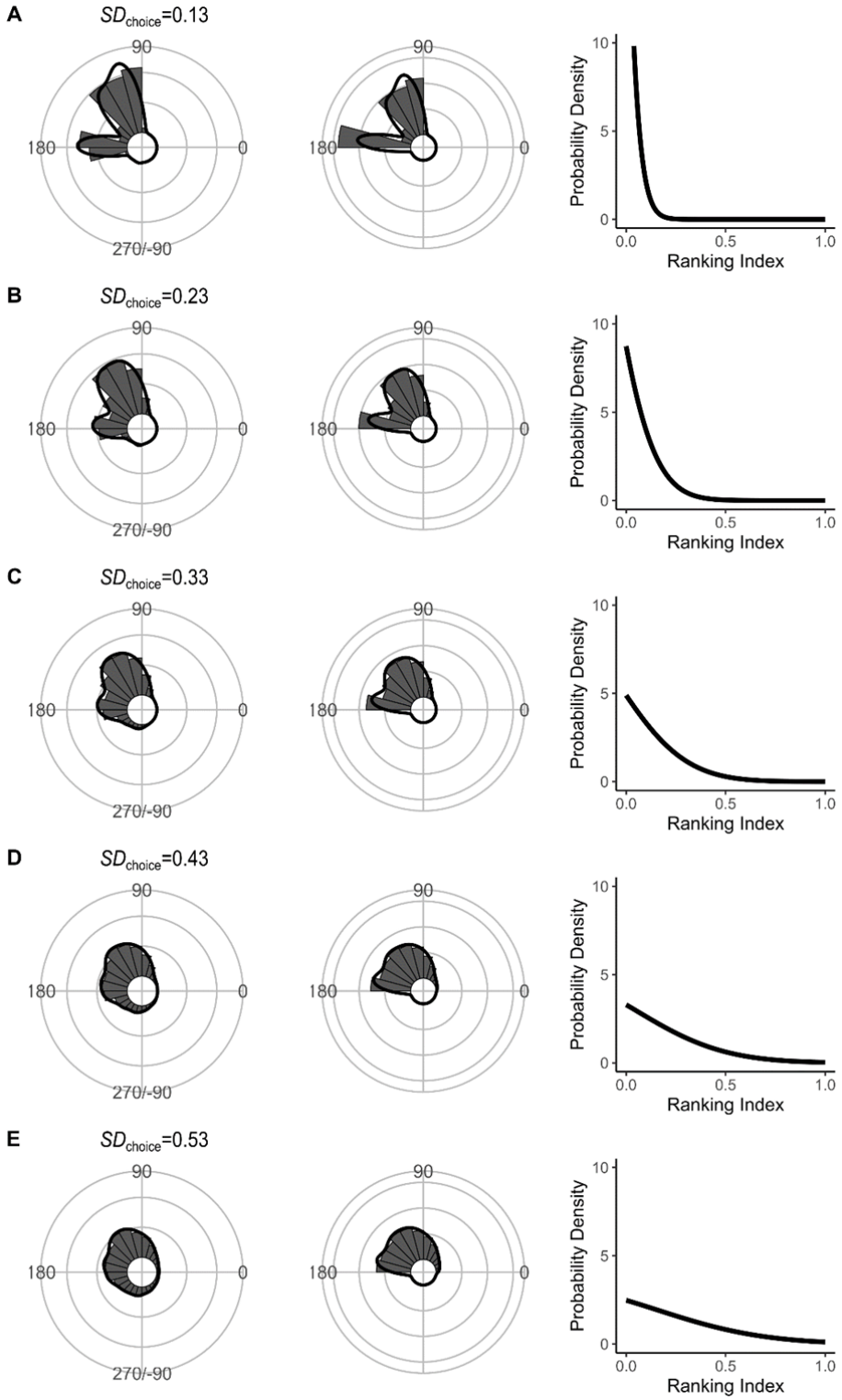

Figure 7—figure supplement 4. Effect of SD_{choice} [s.d. of the truncated normal distribution for ET choice from the continuum of the optimal ET (ranking index=0) and worst ET (ranking index=1)] on the theoretical distribution of escape trajectories (ET, left panel; ET_{semi}, middle panel). Circular histograms of the theoretical escape trajectories were estimated by a Monte Carlo simulation of the geometric model. The other parameter values are the same as the values used for explaining the escape response of *Pagrus major*. The R code is available at Figshare ("Source code 1.R").

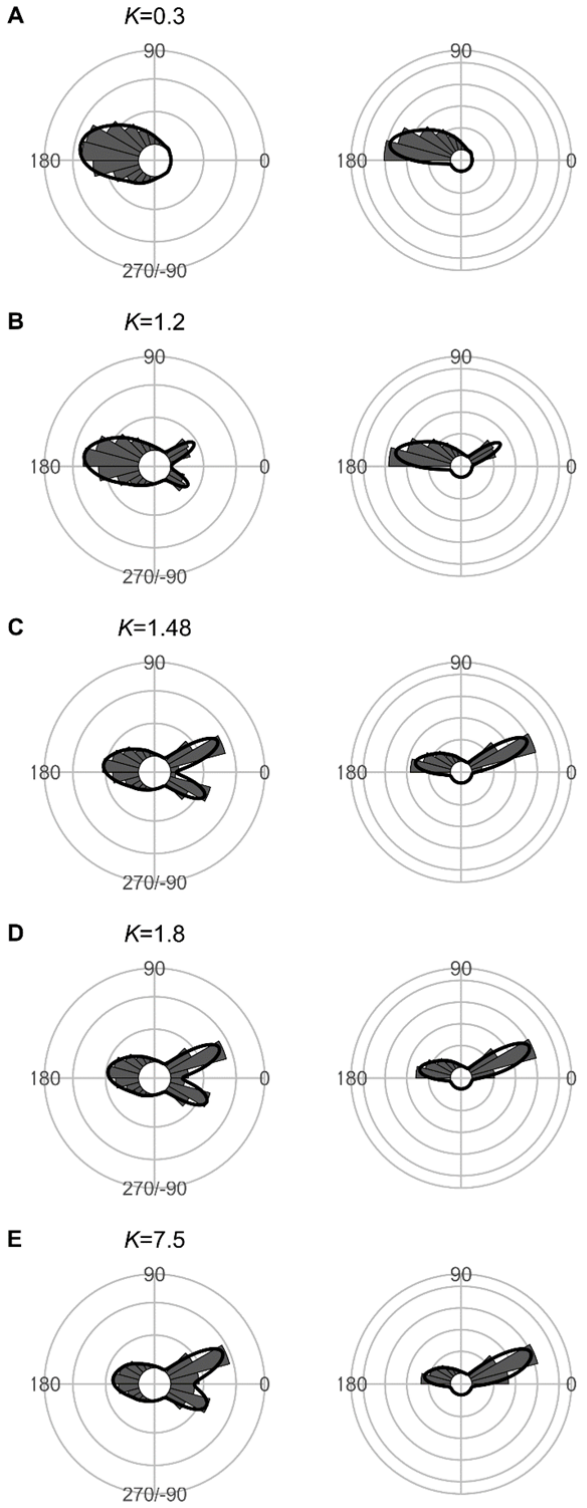

Figure 7—figure supplement 5. Effect of predator speed U_{pred} ($K=U_{pred}/U_{prey}$) on the theoretical distribution of escape trajectories (ET, left panel; ET_{semi}, right panel). Circular histograms of the theoretical escape trajectories were estimated by a Monte Carlo simulation of the geometric model where the predator can adjust its approach path. $D_{initial}$ is 130 mm, D_{react} is 70 mm, R_{turn} is 12 mm, D_{attack} is 400 mm, and the other parameter values are the same as the values used for explaining the escape response of *Pagrus major*. The R code is available at Figshare ("Source code 1.R").

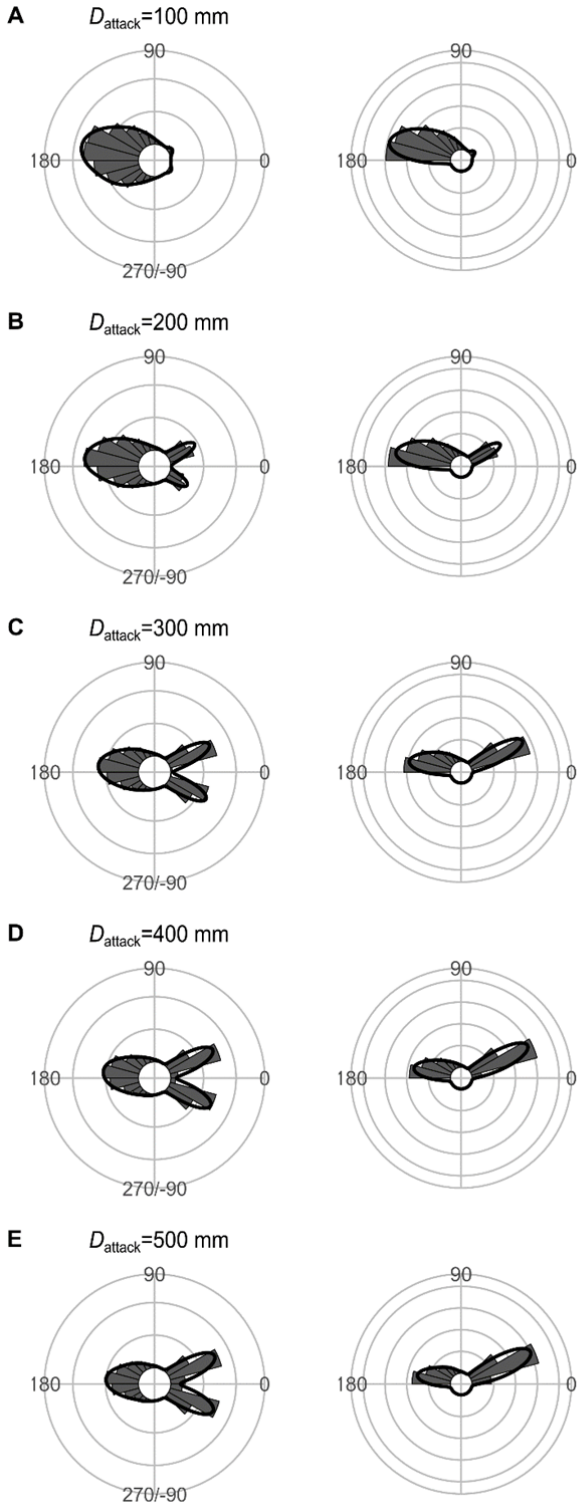

Figure 7—figure supplement 6. Effect of D_{attack} (the distance between the prey's initial position and the endpoint of the predator attack) on the theoretical distribution of escape trajectories (ET, left panel; ET_{semi}, right panel). Circular histograms of the theoretical escape trajectories were estimated by a Monte Carlo simulation of the geometric model where the predator can adjust its approach path. $D_{initial}$ is 130 mm, D_{react} is 70 mm, R_{turn} is 12 mm, and the other parameter values are the same as the values used for explaining the escape response of *Pagrus major*. The R code is available at Figshare ("Source code 1.R").

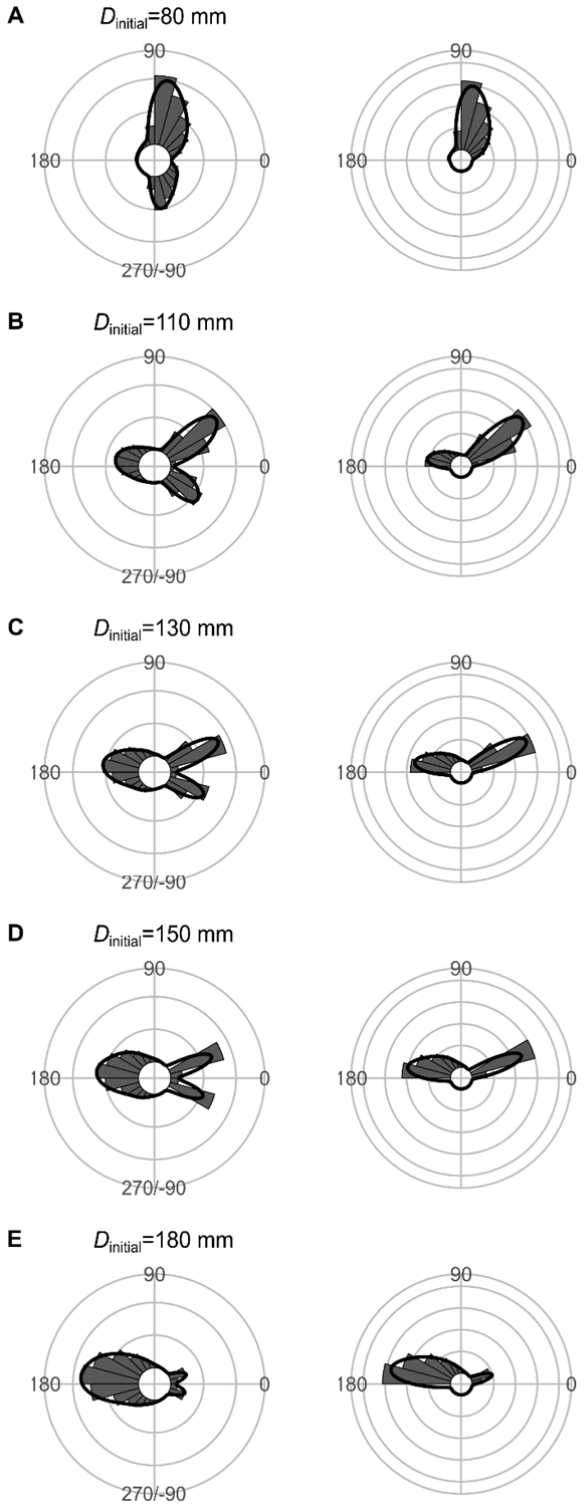

Figure 7—figure supplement 7. Effect of $D_{initial}$ (the distance between the prey and the predator at the onset of the prey's escape response) on the theoretical distribution of escape trajectories (ET, left panel; ET_{semi}, right panel). Circular histograms of the theoretical escape trajectories were estimated by a Monte Carlo simulation of the geometric model where the predator can adjust its approach path. D_{react} is 70 mm, R_{turn} is 12 mm, D_{attack} is 400 mm, and the other parameter values are the same as the values used for explaining the escape response of *Pagrus major*. The R code is available at Figshare ("Source code 1.R").

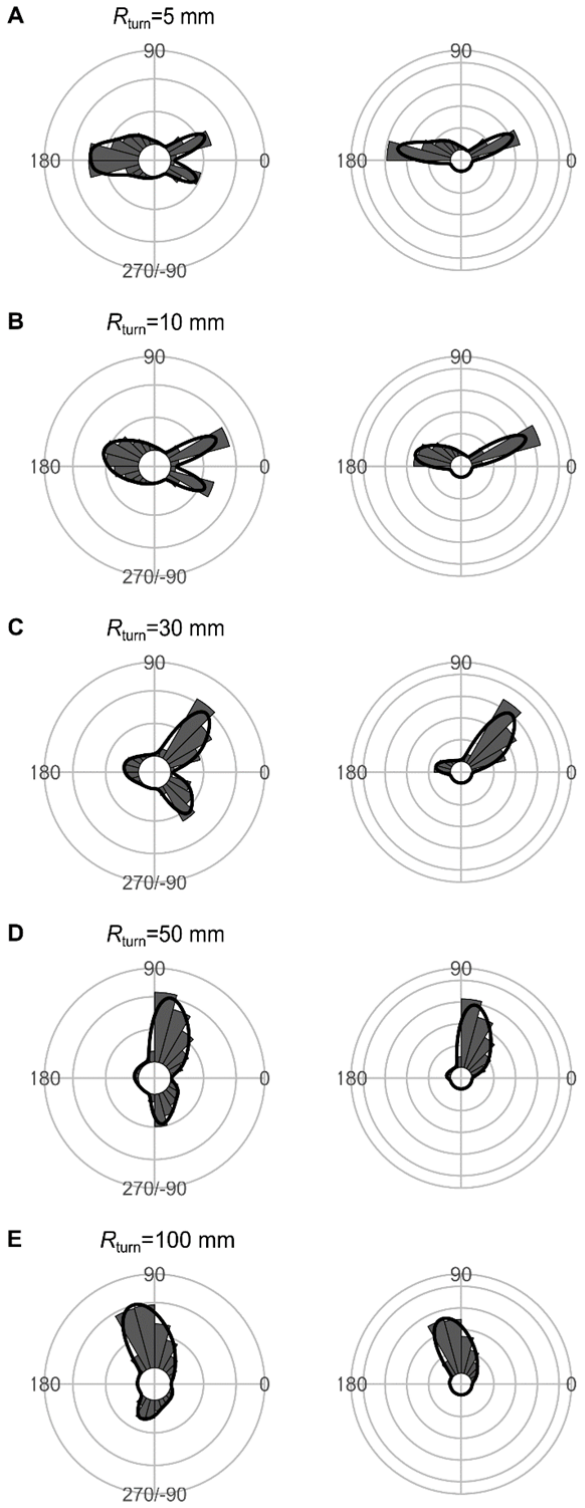

Figure 7—figure supplement 8. Effect of the minimum turning radius of the predator R_{turn} on the theoretical distribution of escape trajectories (ET, left panel; ET_{semi}, right panel). Circular histograms of the theoretical escape trajectories were estimated by a Monte Carlo simulation of the geometric model where the predator can adjust its approach path. $D_{initial}$ is 130 mm, D_{react} is 70 mm, D_{attack} is 400 mm, and the other parameter values are the same as the values used for explaining the escape response of *Pagrus major*. The R code is available at Figshare ("Source code 1.R").

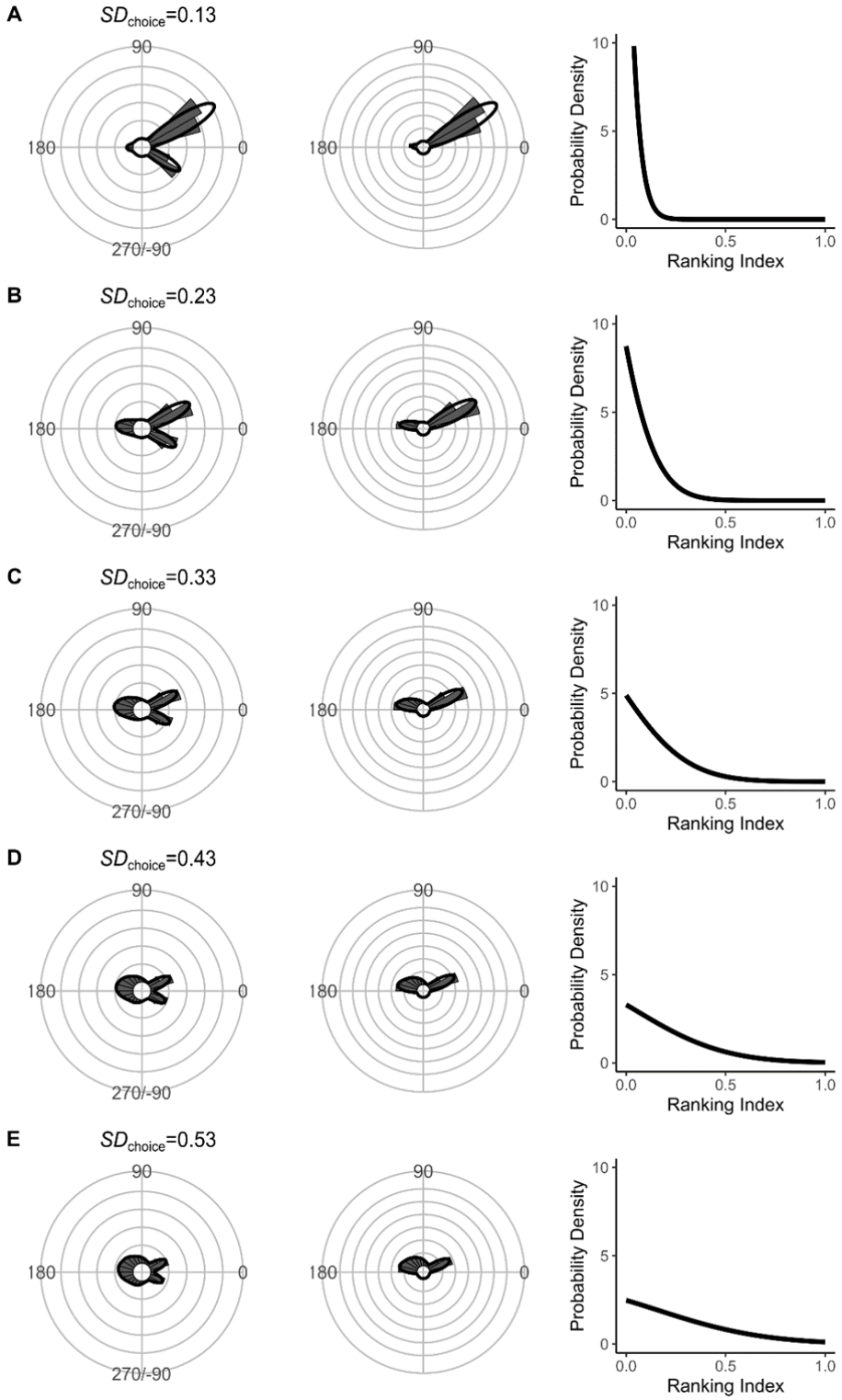

Figure 7—figure supplement 9. Effect of SD_{choice} [s.d. of the truncated normal distribution for ET choice from the continuum of the optimal ET (ranking index=0) and worst ET (ranking index=1)] on the theoretical distribution of escape trajectories (ET, left panel; ET_{semi}, middle panel). Circular histograms of the theoretical escape trajectories were estimated by a Monte Carlo simulation of the geometric model where the predator can adjust its approach path. $D_{initial}$ is 130 mm, D_{react} is 70 mm, D_{attack} is 400 mm, and the other parameter values are the same as the values used for explaining the escape response of *Pagrus major*. The R code is available at Figshare ("Source code 1.R").

1154

Appendix 1

Mathematical formula for the geometric model modified from Corcoran & Conner (2016) [24].

When the prey's center of mass (CoM) at the onset of its escape is located at point (0, 0), the trajectory of the CoM (X_{prey}, Y_{prey}) is given by:

$$\boldsymbol{Y_{\mathrm{prey}} = X_{\mathrm{prey}} \tan(\alpha + \beta)} \quad [1]$$

The edge of the safety zone is determined by the half-width of the predator capture device D_{width}, the distance between the prey and the predator at the onset of the prey's escape response D_{initial}, the distance required for the predator to react the prey's escape response to initiate its turn D_{react}, the distance between the prey's initial position and the tip of the predator capture device at the end of the predator attack D_{attack}, the minimum turning radius of the predator R_{turn}, and the shape of the predator's capture device at the moment of attack, which is approximated as an arc with a certain radius R_{device} (Appendix 1—figure 1B). The edge of the safety zone can be divided into four parts: 1) the straight line before the onset of the predator's turn, 2) the arc of the minimum inner turning radius, 3) the capture device shape at the end of the predator attack when it attacks with the minimum turning radius, 4) the involute curve where the tip of the predator capture device traverses a specific distance from the initial position, which can be described by the trace of unwrapping a taut string from the minimum turning circle (Appendix 1—figure 1B). Note that the model may lack some parts, depending on the values of parameters.

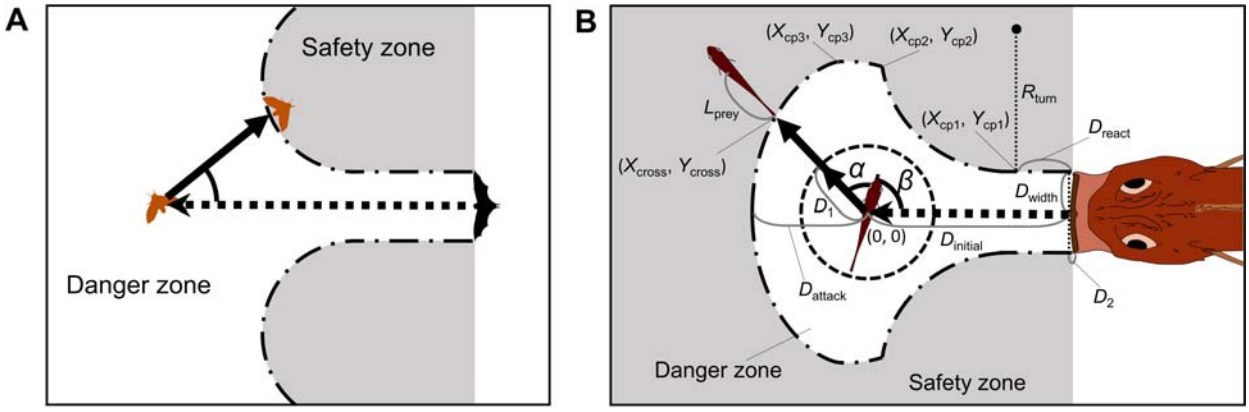

Appendix 1—figure 1. Proposed geometric models for animal escape trajectories. (A) A previous geometric model proposed by Corcoran & Conner (2016) [24]. (B) The geometric model modified from Corcoran & Conner (2016) [24]. Two factors are added to Corcoran's model: the endpoint of the predator attack, and the time required for the prey to turn. See Appendix 1 for details of the definitions of the variables and mathematical formulas.

The projection of the predator's capture device edge along the X-axis D_2 can be expressed as:

$$\boldsymbol{D_2 = R_{device}\{1 - \cos(\sin^{-1}\frac{D_{width}}{R_{device}})\}} \quad [2]$$

The angle for the predator to traverse with the minimum turning radius γ can be expresses as:

$$\boldsymbol{\gamma = \frac{D_{initial} - D_{react} + D_{attack}}{R_{turn}}} \quad [3]$$

The x and y coordinates of the change point between the 1st and 2nd parts of the safety zone edge (X_{cp1}, Y_{cp1}) can be expressed as:

$$\begin{cases} \boldsymbol{X_{cp1} = D_{initial} - D_{react} + D_2} \\ \boldsymbol{Y_{cp1} = D_{width}} \end{cases} \quad [4]$$

The x and y coordinates of the change point between the 2nd and 3rd parts of the safety zone edge (X_{cp2}, Y_{cp2}) can be expressed as:

$$\begin{cases} \boldsymbol{X_{cp2} = D_2\cos\gamma + (D_{width} - R_{turn})\sin\gamma + D_{initial} - D_{react}} \\ \boldsymbol{Y_{cp2} = -D_2\sin\gamma + (D_{width} - R_{turn})\cos\gamma + R_{turn}} \end{cases} \quad [5]$$

The x and y coordinates of the change point between the 3rd and 4th parts of the safety zone edge (X_{cp3}, Y_{cp3}) can be expressed as:

$$\begin{cases} \boldsymbol{X_{cp3} = -R_{turn}\sin\gamma + D_{initial} - D_{react}} \\ \boldsymbol{Y_{cp3} = -R_{turn}\cos\gamma + R_{turn}} \end{cases} \quad [6]$$

The x and y coordinates of the 1st part of the safety zone edge (X_{safe1}, Y_{safe1}) are given by:

$$\boldsymbol{Y_{safe1} = D_{width}} \quad [7]$$

The x and y coordinates of the 2nd part of the safety zone edge (X_{safe2}, Y_{safe2}) are given by:

$$\boldsymbol{(X_{safe2} - D_{initial} + D_{react})^2 + (Y_{safe2} - R_{turn})^2 = D_2{}^2 + (D_{width} - R_{turn})^2} \quad [8]$$

The x and y coordinates of the 3rd part of the safety zone edge (X_{safe3}, Y_{safe3}) are given by:

$$\boldsymbol{(X_{safe3} - D_{initial} + D_{react} - R_{device}\cos\gamma + R_{turn}\sin\gamma)^2} \quad [9]$$

$$\boldsymbol{+ (Y_{safe3} - R_{turn} + R_{device}\sin\gamma + R_{turn}\cos\gamma)^2 = R_{device}{}^2}$$

For calculating the x and y coordinates of the 4th part of the safety zone edge (X_{safe4}, Y_{safe4}), the formula of involute curve from a circle of radius R_{turn} whose center is the origin (0, 0) with a tip of the string at (R_{turn}, 0) is introduced as:

$$\begin{cases} \boldsymbol{x = R_{turn}(\cos\theta + \theta\sin\theta)} \\ \boldsymbol{y = R_{turn}(\sin\theta - \theta\cos\theta)} \end{cases}, \boldsymbol{0 \le \theta \le \gamma} \quad [10]$$

where θ denotes an angle for an unwrapped string from the circle in a counter-clockwise direction. By moving and rotating this point (x, y), we can calculate the 4th part of the safety zone edge (X_{safe4},

Y_{safe4}) as:

$$\begin{cases} \boldsymbol{X_{safe4} = D_{initial} - D_{react} - x\sin\gamma + y\cos\gamma} \\ \boldsymbol{Y_{safe4} = R_{turn} - x\cos\gamma + y\sin\gamma} \end{cases} \quad [11]$$

From equations [1] to [11], the x and y coordinates of the crossing point of the escape path and the safety zone edge (X_{cross}, Y_{cross}) are given by a function of D_{width}, D_{attack}, R_{device}, $D_{initial}$, D_{react}, R_{turn}, and α+β.

The prey can escape from the predator when the time required for the prey to enter the safety zone (T_{prey}) is shorter than the time required for the predator's capture device to reach that entry point (T_{pred}). Therefore, the prey is assumed to maximize the difference between the T_{pred} and T_{prey} (T_{diff}). To incorporate the time required for the prey to turn, T_{prey} was divided into two phases: the fast-start phase, which includes the time for turning and acceleration (T_1), and the constant speed phase (T_2). This assumption is consistent with the previous studies [34-36] and was supported by our experiment (See Figure 4—figure supplement 1). Therefore:

$$\boldsymbol{T_{prey} = T_1 + T_2} \quad [12]$$

For simplicity, the prey was assumed to end the fast-start phase at a certain displacement from the initial position in any α (D_1; the radius of the dotted circle in Appendix 1—figure 1B) and to move at a constant speed U_{prey} to cover the rest of the distance (toward the edge of the safety zone $\sqrt{{X_{cross}}^2 + {Y_{cross}}^2} - D_1$, plus the length of the body that is posterior to the center of mass L_{prey}). Because a larger $|\alpha|$ requires further turning prior to forward locomotion, which takes time [34, 37], and the initial velocity after turning was dependent on $|\alpha|$ in our experiment (See Figure 4B), T_1 is given by a function of $|\alpha|$ [$T_1(|\alpha|)$]. Therefore, T_{prey} can be expressed as:

$$\boldsymbol{T_{prey} = T_1(|\alpha|) + \frac{\sqrt{{X_{cross}}^2 + {Y_{cross}}^2} - D_1 + L_{prey}}{U_{prey}}} \quad [13]$$

When the prey reaches the 1st part of the safety zone edge, T_{pred} can be expressed as:

$$\boldsymbol{T_{pred} = \frac{D_{initial} + D_2 + D_{react} - X_{cross}}{U_{pred}}} \quad [14]$$

When the prey reaches the 2nd part of the safety zone edge, T_{pred} can be expressed as:

$$\boldsymbol{T_{pred}} \quad [15]$$

$$= \frac{\boldsymbol{D_{react} + R_{turn}\tan^{-1}\dfrac{D_2(Y_{cross} - R_{turn}) - (X_{cross} - D_{initial} + D_{react})(D_{width} - R_{turn})}{D_2(X_{cross} - D_{initial} + D_{react}) + (D_{width} - R_{turn})(Y_{cross} - R_{turn})}}}{\boldsymbol{U_{pred}}}$$

When the prey reaches the 3rd or 4th part of the safety zone edge, T_{pred} can be expressed as:

$$\boldsymbol{T_{pred}} = \frac{\boldsymbol{D_{initial}} + \boldsymbol{D_{attack}}}{\boldsymbol{U_{pred}}} \quad [16]$$

From equations [1] to [16], we can calculate T_{diff} in response to the changes of α and β, from D_1, D_{width}, D_{attack}, R_{device}, $D_{initial}$, D_{react}, R_{turn}, U_{prey}, U_{pred}, and $T_1(|\alpha|)$. Given that the escape success is assumed to be dependent on T_{diff}, the theoretically optimal ET can be expressed as:

$$\textbf{The optimal ET} = \underset{\boldsymbol{\alpha+\beta}}{\textbf{argmax}}(\boldsymbol{T_{diff}}) \quad [17]$$